Enzyme-Like Click Catalysis by a Copper-Containing Single-Chain Organic Nanoparticle

Junfeng Chen,† Jiang Wang,‡ Yugang Bai,† Ke Li,† Edzna S. Garcia,† Andrew L. Ferguson,§ and Steven C. Zimmerman*,†

Department of Chemistry, University of Illinois at Urbana-Champaign, Urbana, Illinois 61801, United States

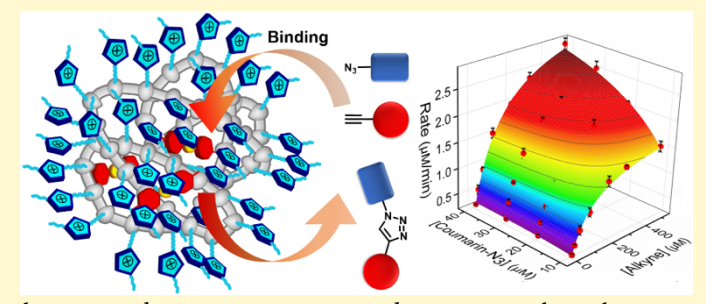
[§]Institute for Molecular Engineering, 5640 South Ellis Avenue, Chicago, Illinois 60637, United States



S Supporting Information

ABSTRACT: A major challenge in performing reactions in biological systems is the requirement for low substrate concentrations, often in the

micromolar range. We report that copper crosslinked single-chain polymeric nanoparticles (SCPNs) are able to significantly increase the efficiency of copper(I)-catalyzed alkyne-azide cycloaddition (CuAAC) reactions at low substrate concentration in aqueous buffer by promoting substrate binding. Using a fluorogenic click reaction and dye uptake experiments, a structure-activity study is performed with SCPNs of different size and copper content and substrates of varying charge and hydrophobicity. The high catalytic efficiency and selectivity is attributed to a mechanism that involves an enzyme-like binding process. Saturation transfer difference



(STD) NMR spectroscopy, 2D-NOESY NMR, kinetic analyses with varying substrate concentration, and computational simulations are consistent with a Michaelis-Menten, two-substrate random sequential enzyme-like kinetic profile. This general approach may prove useful for developing more sustainable catalysts and as agents for biomedicine and chemical biology.

INTRODUCTION

Metalloenzymes often achieve their remarkable catalytic efficiency and selectivity through an architecture that places a substrate binding site in close proximity to a reactive metal center. The result is an enzymatic reaction that is fast, clean, and selective despite the complex and competitive aqueous bioenvironment. The protein scaffold plays a key role in protecting the reactive metal center. Not surprisingly, considerable effort has focused on developing artificial metalloenzymes.1 In parallel, an increasing number of transition metal catalysts have been developed that function in aqueous media, some sufficiently biocompatible to operate inside the competitive environment of living cells.² These advances have exciting implications for sustainable chemistry and as powerful new tools for chemical biology and medicinal chemistry.2d Nonetheless, significant hurdles remain especially in living systems where the required low substrate concentration and physiological pH and temperature often results in low reaction rates. The further demands for low toxicity and compatibility with a broad range of redox-active and coordinating functionality suggests that improvements in catalytic efficiency and biocompatibility may require a protein-like shell for shielding the metal center and for substrate binding.

Recently, there has been intense interest in metal-containing, catalytic, single-chain polymeric nanoparticles (SCPNs) formed by intramolecular crosslinking.3 The cross-linked polymers loosely resemble the folded polypeptide structure of bioactive enzymes. More importantly, the wide array of polymerization methods and cross-linking chemistries available to produce SCPNs opens the door to a remarkably broad range of structures and structural tunability. To date, watersoluble, catalytic SCPNs have been reported for copper(I)-catalyzed alkyne-azide cycloaddition (CuAAC),4 enantio- and diastereo-selective reaction,5 reduction,6 palladium-mediated ketone depropargylation,7 enantio-selective sulfur oxidation8 and phenol hydroxylation9 reactions as well as for living radical polymerization processes.¹⁰ As impressive as these examples are, there have been very limited demonstrations of enzyme-like kinetics11 and only few explorations of the putative hydrophobic binding sites, for example, through structure-activity relationships.12

Our interest in cross-linked polymers as organic nanoparticles¹³ and their host-guest capabilities¹⁴ has led us to study their cell uptake¹⁵ and the possibility of creating selective, nanoscale intracellular catalysts.3 We recently reported a single-chain metal-organic nanoparticle, crosslinked by copper coordination chemistry that effected the well-known CuAAC click reaction¹⁶ at ppm levels of copper, both in water and in mammalian and bacterial cells.4 Herein, we report the synthesis of SCPNs with different structures that has allowed us to develop a structure-activity relationship as well as to shed light on the overall reaction mechanism. The copper containing SCPNs show enzyme-like behavior, in particular substrate binding that increases the reaction rate and selectivity. The results suggest that the high catalytic efficiency of SCPNs may be attributed to their enzyme-like structure. As the first demonstration of dual saturation kinetics, this approach to metalloenzyme-mimicry that combines metal centers and a polymeric scaffold should provide a useful strategy for future catalyst design and development.

[‡]Department of Physics, University of Illinois at Urbana-Champaign, Urbana, Illinois 61801, United States

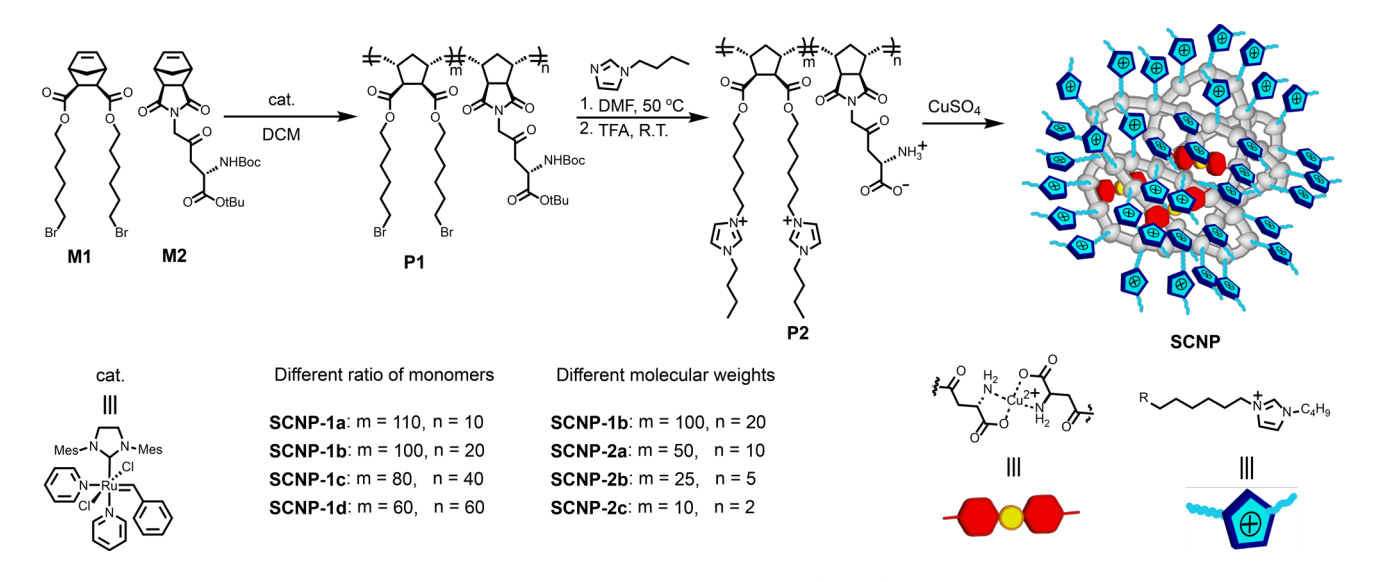


Figure 1. Illustration of the synthesis of the copper crosslinked single-chain organic nanoparticles (SCPNs)

EXPERIMENTAL SECTION

Materials and Instrumentation. Details regarding the chemical reagents used, synthetic procedures for polymers and substrates used in reactions with SCPN catalysts, instrumentation used in this work, and additional details on the computational methods can be found in the Supporting Information.

Procedure for Fluorogenic Click Reactions and Kinetic Analysis. The CuAAC click reaction was monitored using fluorescence-quenched coumarin azide 1 and alkyne 2. ¹⁷ After the click reaction, 1 forms compound 3 with restored fluorescence (Scheme 1). In a 0.7 mL fluorimeter cuvette, SCPNs, sodium ascorbate and a DMSO solution of substrate was added in 0.5 mL PBS buffer at pH = 7.4. The ascorbic acid concentration was 2 mM and the final amount of DMSO was 2% (v/v). The intensity was monitored by fluorimeter every 10 s at λ_{em} = 488 nm with λ_{ex} = 410 nm. The reaction conversion was calculated from the observed fluorescence intensity using pure 3 as the standard. Relative rates were determined as follows. Approximately 1 min after initiating the reaction the increase in fluorescence stabilized and became linear over time. The slope of the fluorescence vs time plot starting at ca. 2 min and using 10-15 data points collected every 10 s was used for the calculation of relative rates.

For kinetic studies, a 4 μM aqueous solution of **SCPN-2a** was used. The concentration of **1** was varied from 10 μM to 40 μM , whereas the concentration of **2** was varied from 12.5 μM to 500 μM due to its higher water solubility. The collected kinetic data was fit to various models but a random sequential two-substrates enzyme kinetics equation gave the best fit. 18

Pyrene Uptake Experiments. The uptake of pyrene as a hydrophobic guest by SCPNs was quantified by shaking a vial containing 0.2 mL of a 1 M pyrene solution in chloroform with 1 mL of a 5 μ M aqueous solution of **SCPN-1b** (or the weight equivalent of other SCPNs). The vial underwent centrifugation and the aqueous layer

removed using a syringe. A UV-vis spectrophotometer was used to measure the absorbance of pyrene in the aqueous layer, a direct measure of the amount solubilized by the SCPN.

STD NMR Method. SCPN-2a was dissolved in D_2O at a concentration of $100~\mu M$, and the substrate was added as a 200~mM DMSO- d_6 solution to reach a final concentration of 2~mM (20 equivalents). Spectra were collected after selectively irradiating SCPN-2a to saturation at δ 1.2 ppm a spectral region where there were no substrate signals. During the saturation period, the magnetization was transferred through intra/intermolecular spin diffusion to other protons on the SCPN as well as to the bound substrates, which further transferred to free molecules due to the exchange of free and bound substrates.

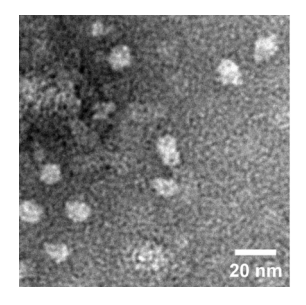
Molecular Dynamics Simulation of SCPN-Substrate Binding. All the SCPN-2a simulations were conducted using the GROMACS 4.6 simulation suite. The binding process was studied with different substrates. The linear polymers were first crosslinked by connecting the copper ions and amino acid groups, and then placed in a 11 nm cubic box of water molecules. The system was simulated at 300 K and 1 bar for 100 ns at which time the SCPN had folded into a stable globular structure. Subsequently 20 copies of one specific substrate molecule were randomly placed into the box and the simulation continued for 20 ns. After discarding the first 10 ns for equilibration, substrate binding was quantified by counting the number of substrate molecules within the nanoparticle over the course of the terminal 10 ns.

RESULT AND DISCUSSION

Synthesis and Characterization of SCPNs. Using a modified procedure based on our original report, P1 were prepared by ring-opening metathesis polymerization (ROMP) of monomers M1 and M2 with pyridine-modified Grubbs third-generation catalyst (Figure 1). Monomer content and degrees of polymerization (DPs) were controlled by adjusting the feed ratios of monomers and the amount of Grubbs catalyst during the ROMP.

Formation of **P1** was confirmed by gel-permeation chromatography (GPC), which showed a good correlation between the measured molecular weights and the catalyst and monomer feed ratios, as well as low polydispersity indices (PDI) that ranged from 1.01 to 1.05. The **P1** were post-functionalized by treatment with *N*-butyl-imidazole providing imidazolium groups that afforded water-soluble, amphiphilic

polymers. Finally, the amino acid residues were deprotected with trifluoroacetic acid (TFA). The resulting **P2** were purified by precipitation in ether followed by dialysis against water. The post-functionalized polymers **P2** were characterized by NMR spectroscopy.



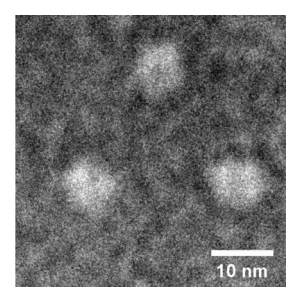


Figure 2. TEM images of SCPN-2a.

Given that several α -amino acids are reported to form stable complexes with Cu(II) and Cu(I) with 2:1 stoichiometries, 22 0.5 eq of $CuSO_4$ relative to the aspartate units was added to **P2** to form Cu(II)-containing SCPN. The resulting nanoparticles were characterized by transmission electron microscopy (TEM) (Figure 2) and dynamic light scattering (DLS, Figure S10). Because of their greater stability, the SCPNs were kept in aqueous solution as Cu(II) complexes. For performing CuAAC click reactions, sodium ascorbate was added to produce the Cu(II) SCPNs in situ.

Rate of CuAAC Reactions and Substrate Selectivity. To test whether substrate charge or hydrophobicity affect the SCPN-catalyzed fluorogenic click reaction, alkyne substrates 4-6 were prepared and mixed with azide 2, SCPN-2a, and ascorbic acid. For comparison, the reactivity of the same substrates was examined using the most highly active tris(triazolylmethyl)amine-based ligand for Cu(I) developed by

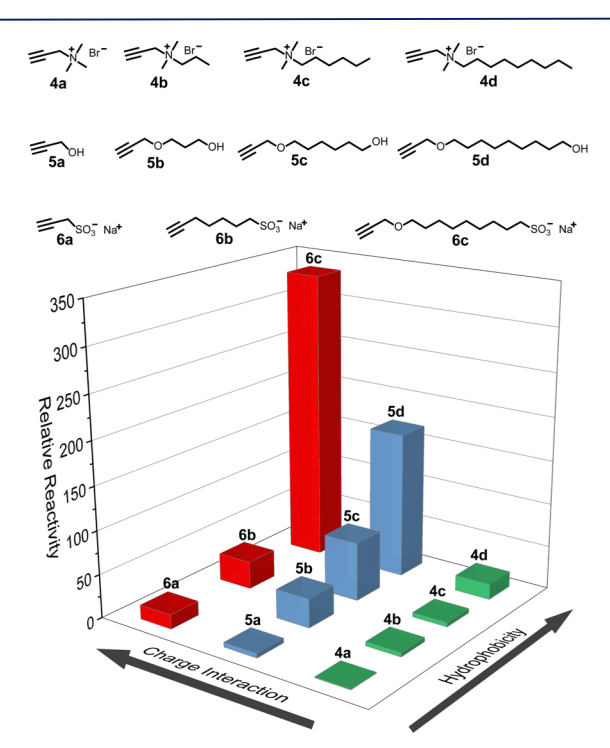


Figure 3. Structures of substrates with hydrophobicity and charge. Fluorogenic reaction rate of different substrates with of **SCPN-2a** (4 μ M), **1** (20 μ M), **4-6** (40 μ M) and sodium ascorbate (2 mM) in PBS buffer pH = 7.4. Rates are relative to that of **4a**.

Liu, Marlowe, Wu, and coworkers known as BTTAA²³ (see Figure S11). In general, **4-6** show only small (<2-fold) rate differences with BTTAA. In contrast, with **SCPN-2a**, along each homologous series of substrates, **4a-4d**, **5a-5d**, and **6a-6c**, the rate of click reaction increased dramatically with increasing length of the aliphatic chain indicating the importance of substrate hydrophobicity (Figure 3). Substrates **4d**, **5d** and **6c** with the longest aliphatic chains were on average 25 times faster than substrates **4a**, **5a** and **6a** with the shortest chains. The importance of hydrophobic binding by the SCPN is further illustrated by the 6-fold rate increase for **6a** seen with **SCPN-2a** relative to BTTAA despite the amino acid-Cu(I) complex being a comparatively poor catalyst.

The other trend evident in the Figure 3 data is that charge significantly influences substrate reactivity. Thus, the click reaction of negatively charged substrate **6c** is two times faster than neutral substrate **5d**, and 20 times faster than cationic substrate **4d**. With BTTAA there is a small advantage for the cationic alkynes **4**, but the largest rate difference (**4a** vs. **6a**) is three-fold and as indicated above, most rates are <2-fold different. The structure activity relationship that emerges from Figure 3 is that polycationic **SCPN-2a** selectively takes up hydrophobic substrates with a preference for anionic over neutral guests whereas an electrostatic repulsion significantly disfavors cationic substrates.

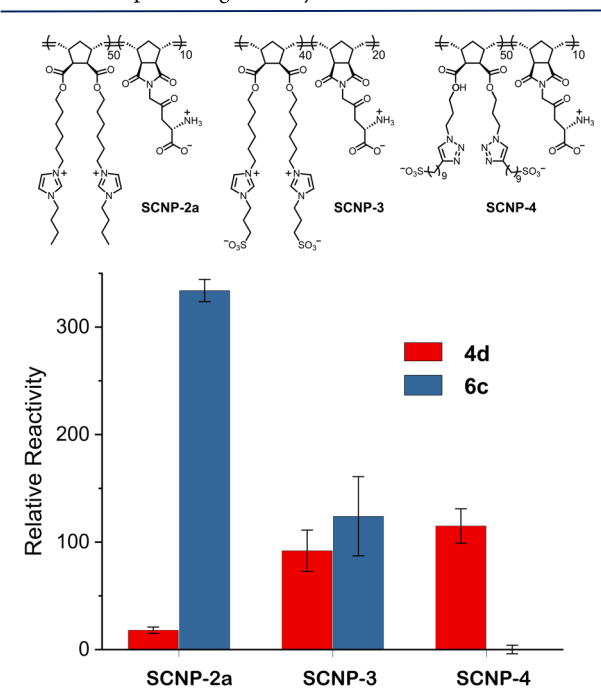


Figure 4. Structure of cationic, zwitterionic, and anionic **SCPNs 2a, 3,** and **4,** respectively and relative reaction rates of substrates **4d** and **6c** in the fluorogenic click reaction. Conditions were **SCPN** ($4\,\mu$ M), **1** ($20\,\mu$ M), **4d** and **6c** ($40\,\mu$ M) and sodium ascorbate ($2\,m$ M) in PBS buffer pH = 7.4. Rates are relative to that of **SCPN-4** with **4d**.

To further study the effect of charge and broaden the substrate selectivity, two additional SCPNs (SCPN-3 and SCPN-4) were prepared (see Figure 4 and Supporting Information). Thus, zwitterionic SCPN-3 and anionic SCPN-4 were designed to test whether the substrate preference in Figure 3 could be altered. Their catalytic performance in the fluorogenic CuAAC reaction was tested with cationic alkyne 4d and anionic alkyne 6c and compared to that with SCPN-2a. As shown in Figure 4, SCPN-4 processed cationic alkyne 4d significantly faster than did SCPN-2a whereas almost no reaction was measured with 6c which reversed the selectivity profile of SCPN-2a. On the other hand, the zwitterionic SCPN-3 exhibited similar rates towards both cationic and anionic substrates.

The SCPN is critical for the catalysis observed. Thus, BTTAA was used to test the role of the polymer in the control experiments (Figure

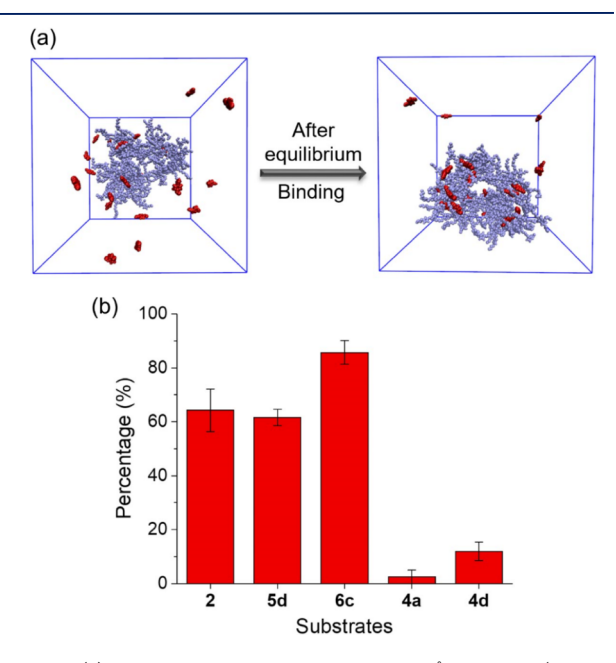


Figure 5. (a) Snapshot of **SCPN-2a** and **2** in an 11 Å water box (water not shown) before and after equilibrium. Polymer atoms were colored as blue, substrate molecule were colored red and solvent molecules were turned off. (b) Percentage of substrate molecules within the nanoparticle averaged over the terminal 10 ns of the simulation. Error bars represent standard deviations of the percentage measured in the equilibrium portion.

S11) because no reaction could be observed with the copper complex of glycine. The data presented in Figures 3 and 4 suggest clearly that one key role played by the polymeric nanoparticle is in binding the substrates in proximity to the metal catalyst. To obtain more than inferential support for the substrate binding model, we examined the binding both computationally and experimentally.

Molecular Dynamics Simulation of Substrate Binding Within SCPN. The potential binding process was studied by molecular dynamics simulation (see Experimental Section and Supporting Information for additional details). When the SCPN-2a structure was built and modeled computationally, it was found to adopt a globular shape with a diameter of ca. 5-6 nm. The substrate-nanoparticle interaction was evaluated by calculating the percentage of small molecules that reside inside the nanoparticle. As shown in Figure 5 and Supporting Movie 1, coumarin azide 2 is mostly bound and differential substrate uptake was observed for 4a, 4d, 5d, and 6c that is consistent with the dependence on the hydrophobicity and charge seen experimentally in Figure 3.

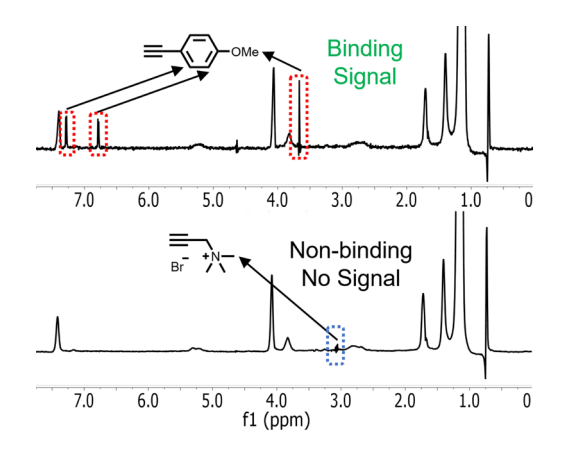


Figure 6. STD spectrums for SCPN-2a (100 μ M) with 2 (2 mM) or 4a (2mM) in D₂O.

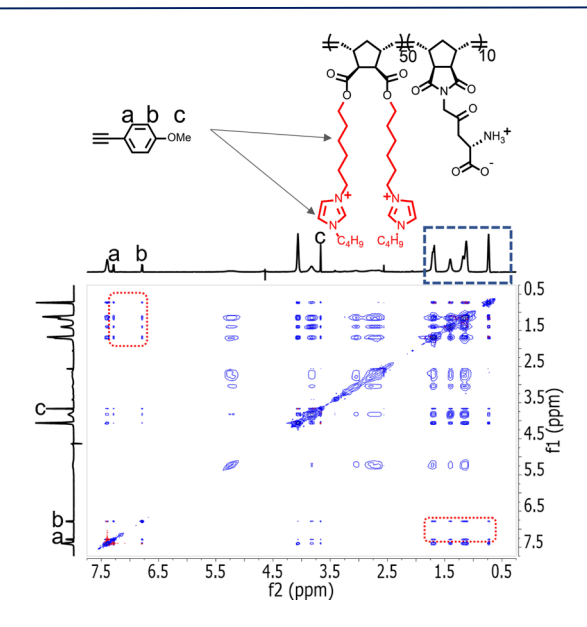


Figure 7. 2D-NOESY spectrum of SCPN-2a (100 μM) with 2 (2 mM) in D₂O.

Substrate Binding is Detected by NMR. To obtain direct experimental evidence of substrate binding, saturation transfer difference (STD) spectroscopy was applied to **SCPN-2a** and alkynes **2** and **4a** to observe possible nuclear Overhauser effect (NOE) between catalyst and substrate. STD has been commonly used to study the interaction between proteins and guest ligands. STD spectra were measured separately for 20 equivalents of **2** and **4a** mixed with **SCPN-2a**. As shown in Figure 6, the hydrophobic substrate **2** exhibited relatively strong signals indicating residence within the polymeric nanoparticle. In contrast, the positively charged and hydrophilic substrate **4a** showed negligible signal. These results support substrate binding and are consistent with the observed reaction kinetics.

The binding between substrate **2** and **SCPN-2a** was further elucidated by two-dimensional nuclear Overhauser effect spectroscopy (2D-NOESY). As seen in Figure 7, substrate **2** gives signals at δ 7.3, 6.8, and 3.7 ppm all three of which exhibit strong cross-peaks to SCPN peaks appearing between δ 0.5 - 2.0 ppm. This region contains the signals of

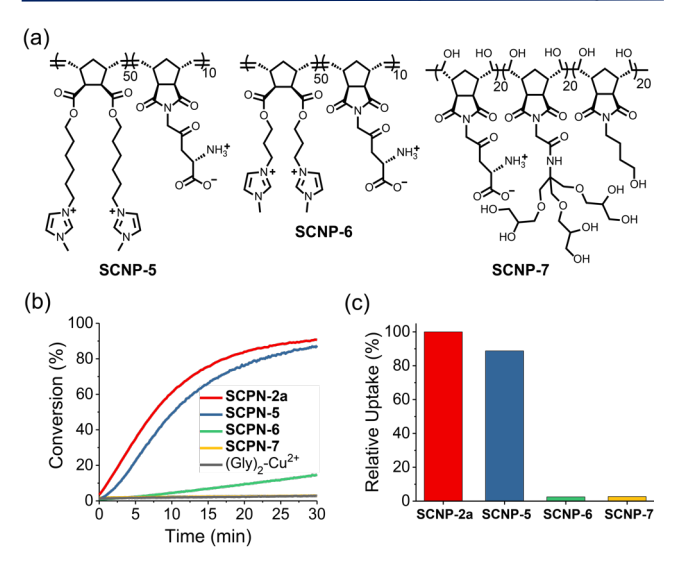


Figure 8. (a) Polymer parent structures of SCPNs with different water solubilization structure. (b) Reaction kinetics of SCPNs with SCPNs (4 μ M), 1 (20 μ M), 2 (40 μ M) and sodium ascorbate (2 mM) in PBS buffer pH = 7.4. (c) Relative pyrene uptake ability.

hydrophobic aliphatic chains. In contrast, the alkene region from the polymer backbone showed almost no NOE signal although it is also hydrophobic. These results suggest that hydrophobic substrates may preferentially bind within pockets formed by the aliphatic side-chains and the imidazolium groups.

Probing the Importance of the SCPN Size, Copper Content, and Amphiphilic Structure. If hydrophobic binding by the amphiphilic sidechains of the SCPN is important to the catalysis then changing the ratio of the aliphatic to imidazolium content within the side-chains would be expected to alter the rate of the click reaction. Thus, SCPN-5 and SCPN-6 were designed with progressively shorter aliphatic chains but otherwise a structure directly analogous to SCPN-2a (Figure 8a). A neutral, but very hydrophilic nanoparticle (SCPN-7) was also prepared.

To have a more quantitative measure of the SCPN's ability to bind hydrophobic substrates, pyrene uptake experiments were performed, where the percent of pyrene extracted from chloroform into the aqueous layer provides a direct measure of the ability of the SCPN to bind a hydrophobic substrate. As seen in Figure 8b and 8c, there is an excellent correlation between catalytic activity and the ability of the SCPN to take up pyrene. Replacing the butyl group to methyl minimally decreases the rate of the click reaction and the pyrene uptake (compare SCPN-2a and SCPN-5) suggesting that the peripheral butyl groups minimally participate in binding and catalysis. In contrast, SCPN-6 and SCPN-7, show little binding and little catalysis. It is likely that these two polymeric nanoparticles are too hydrophilic to significantly bind substrate.

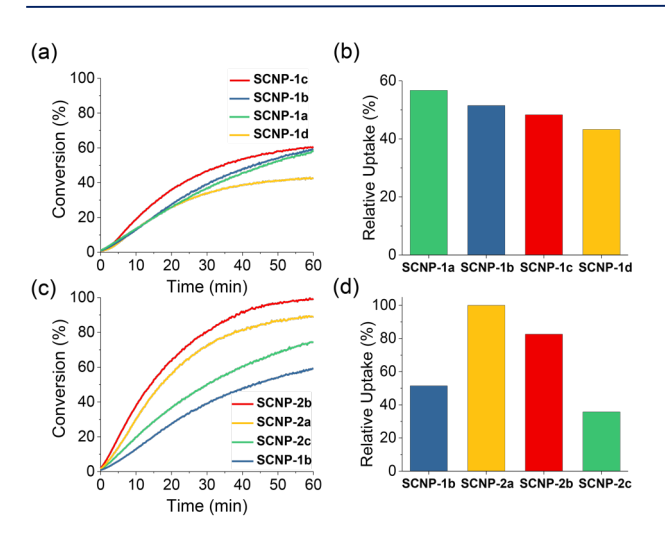


Figure 9. (a) Rate of fluorogenic CuAAC click reactions performed with 1 (20 μ M), 2 (40 μ M), sodium ascorbate (2 mM) and 1 μ M SCPN. (b) Pyrene uptake by SCPN. (d) Fluorogenic CuAAC click reaction performed with 1 (20 μ M), 2 (40 μ M), sodium ascorbate (2 mM) and 1 μ M **SCPN-1b**. Other SCPN run at same mass concentration. (d) Pyrene uptake by SCPN. Pyrene uptake by **SCPN-2a** was set at 100% relative uptake here and (b).

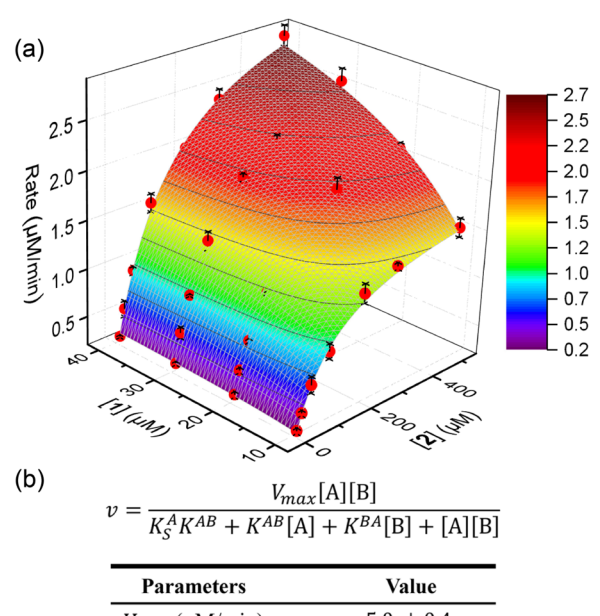
As seen in Figure 1, four nanoparticles, **SCPN-1a-d**, were prepared with roughly the same degree of polymerization but different **M1** to **M2** ratios. An increase in the **M2:M1** ratio increases both the crosslinking density and the number of copper complexes per SCPN. To determine the role of these two variables, the rate of the fluorogenic CuAAC click reaction was measured at 1 µM of each SCPN. Using a constant SCPN concentration means that the solution of **SCPN-1d** contained six times more copper than did **SCPN-1a**. As seen in Figure 9a, the reaction rates of all four SCPN were very similar. Despite **SCPN-1d** containing the largest amount of copper ion, it showed the slowest rate. Dye uptake experiments were also conducted and as shown in Figure 9b. The four SCPNs exhibited comparable results, each SCPN solubilizing the hydrophobic pyrene structure in water between 43-57% of that solubilized by **SCPN-2a**. The increased copper content is expected to be accompanied by a more tightly cross-linked and more polar polymer

interior and this is reflected in the regular, albeit small, decrease in pyrene uptake. Overall, the results suggest that the copper content is less important than the SCPN capacity for hydrophobic binding.

The same general approach was used to determine the importance of nanoparticle size, the size decreasing along the series SCPN-1b < SCPN-2a < SCPN-2b < SCPN-2c (Figure 9c and 9d). The dye uptake experiments were performed at the same mass concentrations. SCPN size appears to matter more than copper content, although the effect both on rate and pyrene uptake is not large. The results are again consistent with the rate correlating with SCPN pyrene uptake and further suggesting that intermediate sized SCPN will give the fastest catalysts. It is possible that small polymers might not have enough flexibility to form hydrophobic pockets whereas large polymers might pack too tightly.

Enzyme-Mimetic Behavior by SCPNs as Revealed by Kinetic Analysis. Given that the combined results of the STD, 2D-NOESY, and pyrene uptake experiments, suggest that the SCPNs catalyze the CuAAC click reaction by binding the azide and alkyne in proximity to the metal catalytic site, we sought to apply enzyme kinetics to the SCPN-2a catalyzed CuAAC click reaction of 1 and 2. Because the CuAAC click reaction is a two-substrate reaction that requires binding of both substrates in random sequence, the kinetics data were analyzed using the random-sequential Bi-Bi model.¹⁸

By varying both substrate concentrations and measuring the rate of the CuAAC click reaction between 1 and 2, a three-dimensional rate surface was generated as shown in Figure 10. Looking along each concentration axis separately, i.e., holding one component constant and increasing the other, it can be seen that the reaction rate gradually reaches saturation, consistent with Michaelis-Menton-like kinetics. The surface in Figure 9 could be fit to the equation describing a random-sequential Bi-Bi model with the R-square as high as 0.99. Palmans, Meijer, and coworkers have reported¹¹ one of the few examples of Michaelis-Menten kinetics, but to our knowledge, this represents the



Parameters	Value
V_{max} (μ M/min)	5.0 ± 0.4
K_S^A (μ M)	52 ± 32
K^{AB} (μ M)	18 ± 3.6
K^{BA} (μ M)	178 ± 34
R-Square	0.99

Figure 10. (a) Random-sequential two substrates enzyme kinetics equation fitting of **SCPN-2a** kinetics data. (b) Fitting equation and parameters.

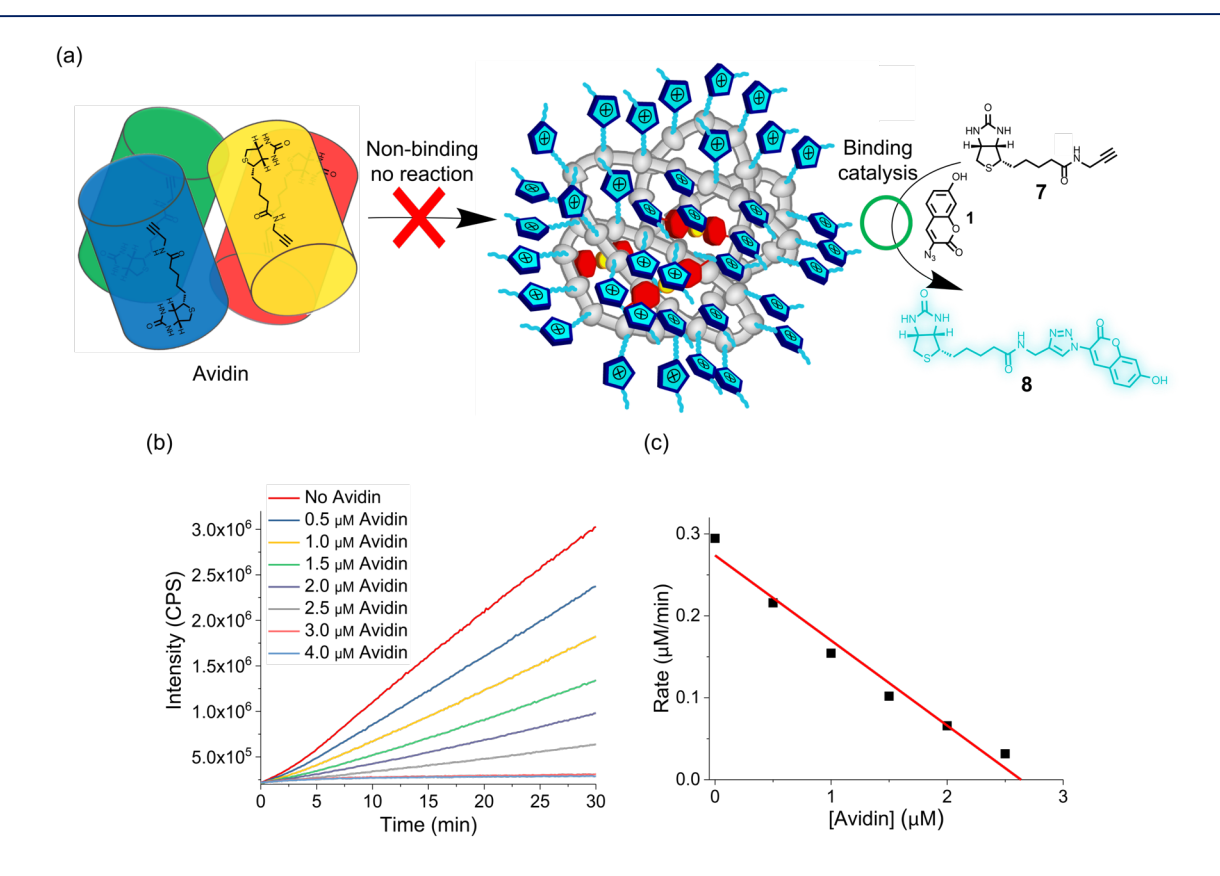


Figure 11. (a) Illustration of selective catalysis on free substrates by SCPNs. (b) Fluorogenic CuAAC click reaction on 7 (10 μ M) with SCPN-2a (4 μ M) at different avidin concentration in PBS buffer pH=7.4. (c) Reaction rate over the concentration of avidin.

first demonstration of two substrate enzyme kinetic behavior for an SCPN-based catalyst.

Toward The Use of SCPN in Bioapplications. We previously demonstrated that copper-containing SCPN could perform click reactions both in bacterial and mammalian cells. Here the interest was in exploring the potential use of SCPN in an additional application. As supported by the results above, substrate binding is the key step during the catalysis performed by the SCPN. If the substrate has a higher binding affinity toward another macro-molecular scaffold and is deeply buried inside a binding pocket, the reactive group on the substrate would be unreactive toward the SCPN because of the steric effect of the polymeric structure. Thus, free molecules would readily undergo the click transformation whereas bound molecules would not. Such an approach might provide a simple click-based alternative to fragment based drug discovery.²⁵

To test the general principle of binding-inhibited SCPN-click, biotin and avidin was chosen because of its strong noncovalent binding, relatively buried binding site, and utility in a range of applications. ²⁶ Each avidin molecule offers four binding sites (Figure 11). Alkyne substrate **7** was prepared with a short linker to the biotin unit, which ensures the alkyne group will be deeply buried inside the protein (Supporting Information). During the fluorogenic click reaction, the concentrations of **SCPN-2a**, **1** and **7** were kept constant, and reaction kinetics were measured with increasing concentration of avidin. Thus, the concentration of free **7** that is accessible to the nanoparticle progressively decreased with a concomitant reduction in reaction rate that is linearly correlated with the avidin concentration (Figure 11c) consistent with the experimental design.

CONCLUSION

Copper crosslinked single-chain organic nanoparticles were designed and synthesized with cationic, anionic, zwitterion, and neutral

water-solubilizing groups. By using alkyne substrates with different charges and varying alkyl chain length, a structure-activity relationship was developed. In addition, the size of the polymeric nanoparticle and number of copper centers per particle were varied. The overall picture that emerges is that the rate of the copper-containing SCPN is governed primarily by the hydrophobic character of the substrate and polymer and the charge complementarity. The other factors appear to be less critical although an intermediate-sized polymer appears to have some advantages over larger and smaller SCPNs.

The structure-activity relationship combined with the STD spectroscopy, 2D-NOESY, and computational experiments strongly support the binding of both the alkyne and azide as critical for providing the enhanced rate and substrate selectivity. Indeed, the synthetic single-chain nanoparticle catalysts exhibited two-substrate enzyme kinetics behavior, making the analogy to a metalloenzyme apt. Model studies with avidin and alkyne-labeled biotin show the potential use of SCPN in drug discovery. We are actively working on extending this system to other metal centers, and modifying the macromolecular scaffolds to afford greater rate enhancements for biolabeling both *in vitro* and *in cellulo* and the results of these efforts will be report in due course.

ASSOCIATED CONTENT

Supporting Information.

The Supporting Information is available free of charge on the ACS Publications website at DOI:

General experimental procedures and detailed synthetic procedures and characterization data for small molecules and polymers, and additional kinetic data along with details of the computational methods (PDF)

AUTHOR INFORMATION

Corresponding Author

*sczimmer@illinois.edu

ORCID

Junfeng Chen: 0000-0002-7100-0839 Yugang Bai: 0000-0002-9834-7517 Ke Li: 0000-0003-3851-7710

Edzna S. Garcia: 0000-0003-4935-4988 Steven C. Zimmerman: 0000-0002-5333-3437

Notes

The authors declare no competing financial interest.

ACKNOWLEDGMENT

This work was supported by the National Science Foundation (NSF CHE-1709718) and the Binational Science Foundation (2014116).

REFERENCES

- (1) For lead references see: (a) Ilie, A.; Reetz, M. T. *Isr. J. Chem.* **2015**, *55*, 51–60. (b) Schwizer, F.; Okamoto, Y.; Heinisch, T.; Gu, Y.; Pellizzoni, M. M.; Lebrun, V.; Reuter, R.; Köhler, V.; Lewis, J. C.; Ward, T. R. *Chem. Rev.* **2018**, *118*, 142–231.
- (2) Selected lead reviews: (a) Sasmal, P. K.; Streu, C. N.; Meggers, E. Chem. Commun. 2013, 49, 1581–1587. (b) Chankeshwara, S. V.; Indrigo, E.; Bradley, M. Curr. Opin. Chem. Biol. 2014, 21, 128–135. (c) Yang, M. Y.; Li, J.; Chen, P. R. Chem. Soc. Rev. 2014, 43, 6511–6526. (d) Bai, Y.; Chen, J.; Zimmerman, S. C. Chem. Soc. Rev. 2018, 47, 1811–1821. (e) Martinez–Calvo, M.; Mascarenas, J. L. Coord. Chem. Rev. 2018, 359, 57–79.
- (3) (a) Gonzalez-Burgos, M.; Latorre-Sanchez, A.; Pomposo, J. A. Chem. Soc. Rev. 2015, 44, 6122–6142. (b) Altintas, O.; Barner-Kowollik, C. Macromol. Rapid Commun. 2016, 37, 29–46. (c) Mavila, S.; Eivgi, O.; Berkovich, I.; Lemcoff, N. G. Chem. Rev. 2016, 116, 878–961. (d) Rubio-Cervilla, J.; González, E.; Pomposo, J. Nanomater. 2017, 7, 341–360.
- (4) (a) Bai, Y.; Feng, X.; Xing, H.; Xu, Y.; Kim, B. K.; Baig, N.; Zhou, T.; Gewirth, A. A.; Lu, Y.; Oldfield, E.; Zimmerman, S. C. *J. Am. Chem. Soc.* **2016**, *138*, 11077–11080.
- (5) Huerta, E.; Genabeek, B. v.; Stals, P. J. M.; Meijer, E. W.; Palmans, A. R. A. *Macromol. Rapid Commun.* **2014**, *35*, 1320–1325.
- (6) Terashima, T.; Mes, T.; De Greef, T. F. A.; Gillissen, M. A. J.; Besenius, P.; Palmans, A. R. A.; Meijer, E. W. *J. Am. Chem. Soc.* **2011**, *133*, 4742–4745.
- (7) Liu, Y.; Pauloehrl, T.; Presolski, S. I.; Albertazzi, L.; Palmans, A. R. A.; Meijer, E. W. *J. Am. Chem. Soc.* **2015**, *137*, 13096–13105.
- (8) Zhang, Y.; Tan, R.; Gao, M.; Hao, P.; Yin, D. Green Chem. 2017, 119, 1182–1193.
- (9) Thanneeru, S.; Duay, S. S.; Jin, L.; Fu, Y.; Angeles-Boza, A. M.; He, J. *ACS Macro. Lett.* **2017**, *6*, 652–656.
- (10) (a) Sanchez-Sanchez, A.; Arbe, A.; Kohlbrecher, J.; Colmenero, J.; Pomposo, J. A. *Macromol. Rapid Commun.* **2015**, *36*, 1592–1597. (b) Azuma, Y.; Terashima, T.; Sawamoto, M. *ACS Macro. Lett.* **2017**, *6*, 830–835.
- (11) Huerta, E.; Stals, P. J. M.; Meijer, E. W.; Palmans, A. R. A. Angew. Chem. Int. Ed. 2013, 52, 2906–2910.

- (12) (a) Artar, M.; Souren, E. R. J.; Terashima, T.; Meijer, E. W.; Palmans, A. R. A. ACS Macro. Lett. **2015**, *4*, 1099–1103. (b) Stals, P. J. M.; Cheng, C.-Y.; van Beek, L.; Wauters, A. C.; Palmans, A. R. A.; Han, S.; Meijer, E. W. Chem. Sci. **2016**, *7*, 2011–2015.
- (13) (a) Wendland, M. S.; Zimmerman, S. C. *J. Am. Chem. Soc.* **1999**, *121*, 1389–1390. (b) Schultz, L. G.; Zhao, Y.; Zimmerman, S. C. *Angew. Chem. Int. Ed.* **2001**, *40*, 1962–1966. (c) Lemcoff, N. G.; Spurlin, T. A.; Gewirth, A. A.; Zimmerman, S. C.; Beil, J. B.; Elmer, S. L.; Vandeveer, H. G. *J. Am. Chem. Soc.* **2004**, *126*, 11420–11421. (d) Bai, Y.; Xing, H.; Vincil, G. A.; Lee, J.; Henderson, E. J.; Lu, Y.; Lemcoff, N. G.; Zimmerman, S. C. *Chem. Sci.* **2014**, *5*, 2862–2868.
- (14) (a) Zimmerman, S. C.; Wendland, M. S.; Rakow, N. A.; Zharov, I.; Suslick, K. S. *Nature* **2002**, *418*, 399–403. (b) Zimmerman, S. C.; Quinn, J. R.; Burakowska, E.; Haag, R. *Angew. Chem. Int. Ed.* **2007**, *46*, 8164–8167. (c) Burakowska, E.; Quinn, J. R.; Zimmerman, S. C.; Haag, R. *J. Am. Chem. Soc.* **2009**, *131*, 10574–10580.
- (15) (a) Bai, Y.; Xing, H.; Wu, P.; Feng, X.; Hwang, K.; Lee, J. M.; Phang, X. Y.; Lu, Y.; Zimmerman, S. C. *ACS Nano* **2015**, *9*, 10227–10236. (b) Li, Y.; Bai, Y.; Zheng, N.; Liu, Y.; Vincil, G. A.; Pedretti, B. J.; Cheng, J.; Zimmerman, S. C. *Chem. Commun.* **2016**, *52*, 3781–3784.
- (16) (a) Rostovtsev, V. V.; Green, L. G.; Fokin, V. V.; Sharpless, K. B. *Angew. Chem. Int. Ed.* **2002**, *41*, 2596–2599. (b) Tornoe, C. W.; Christensen, C.; Meldal, M. *J. Org. Chem.* **2002**, *67*, 3057–3064.
- (17) (a) Sivakumar, K.; Xie, F.; Cash, B. M.; Long, S.; Barnhill, H. N.; Wang, Q. Org. Lett. **2004**, *6*, 4603–4606. (b) Zhou, Z.; Fahrni, C. J. J. Am. Chem. Soc. **2004**, *126*, 8862–8863. (c) Le Droumaguet, C.; Wang, C.; Wang, Q. Chem. Soc. Rev. **2010**, *39*, 1233–1239.
- (18) (a) Cleland, W. W. Biochim. Biophys. Acta 1963, 67, 104–137. (b) Ivanetich, K. M.; Goold, R. D. Biochim. Biophys. Acta, Protein Struct. Mol. Enzymol. 1989, 998, 7–13.
- (19) (a) Diederich, F.; Dick, K. J. Am. Chem. Soc. 1984, 106, 8024–8036.
 (b) Denti, T. Z. M.; vanGunsteren, W. F.; Diederich, F. J. Am. Chem. Soc. 1996, 118, 6044–6051.
 (c) Basu Ray, G.; Chakraborty, I.; Moulik, S. P. J. Coll. Interf. Sci. 2006, 294, 248–254.
- (20) Abraham, M. J.; Murtola, T.; Schulz, R.; Páll, S.; Smith, J. C.; Hess, B.; Lindahl, E. *SoftwareX* **2015**, *1*, 19–25.
- (21) Choi, T.-L.; Grubbs, R. H. Angew. Chem. Int. Ed. 2003, 115, 1785–1788.
- (22) (a) Van Heeswijk, W. A. R.; Eenink, M. J. D.; Feijen, J. *Synthesis* **1982**, *1982*, 744–747. (b) Thomas, G.; Zacharias, P. S. *Polyhedron* **1985**, *4*, 811–816. (c) Cerda, B. A.; Wesdemiotis, C. *J. Am. Chem. Soc.* **1995**, *117*, 9734–9739.
- (23) (a) Soriano del Amo, D.; Wang, W.; Jiang, H.; Besanceney, C.; Yan, A. C.; Levy, M.; Liu, Y.; Marlow, F. L.; Wu, P. *J. Am. Chem. Soc.* **2010**, *132*, 16893–16894. (b) Besanceney-Webler, C.; Jiang, H.; Zheng, T.; Feng, L.; Soriano del Amo, D.; Wang, W.; Klivansky, L. M.; Marlow, F. L.; Liu, Y.; Wu, P. *Angew. Chem. Int. Ed.* **2011**, *50*, 8051–8056. (c) See also: Hong, V.; Presolski, S. I.; Ma, C.; Finn, M. G. *Angew. Chem. Int. Ed.* **2009**, *48*, 9879–9883.
- (24) (a) Mayer, M.; Meyer, B. *Angew. Chem. Int. Ed.* **1999**, *38*, 1784–1788. (b) Mayer, M.; Meyer, B. *J. Am. Chem. Soc.* **2001**, *123*, 6108–6117.
- (25) Selected lead reviews: (a) Kolb, H. C.; Sharpless, K. B. *Drug Discov. Today* **2003**, *8*, 1128–1137. (b) Lipinski, C.; Hopkins, A. *Nature* **2004**, *432*, 855–861. (c) Hajduk, P. J.; Greer, J. *Nat. Rev. Drug Discov.* **2007**, *6*, 211–219.
- (26) (a) Wilchek, M.; Bayer, E. A. *Method Enzym.* **1990**, *184*, 14–45. (b) DeChancie, J.; Houk, K. N. *J. Am. Chem. Soc.* **2007**, *129*, 5419–5429. (c) Laitinen, O. H.; Nordlund, H. R.; Hytonen, V. P.; Kulomaa, M. S. *Trends Biotechnol.* **2007**, *25*, 269–277.

Enzyme-Like Click Catalysis by a Copper-Containing Single-Chain Nanoparticle

Junfeng Chen,† Jiang Wang,‡ Yugang Bai,† Ke Li,† Edzna S. Garcia,† Andrew L. Ferguson,§ and Steven C. Zimmerman*,†

Table of contents:

Materials and instruments·····	
iviateriais and instruments	2
Synthesis procedures·····	
Polymer and nanoparticle Characterization······	
	12
Kinetics ·····	·· 17
ITC study ·····	·· 19
Molecular dynamics simulation methods · · · · · · · · · · · · · · · · · · ·	20
References ······	21

[†]Department of Chemistry, University of Illinois at Urbana–Champaign, Urbana, Illinois 61801, United States [‡]Department of Physics, University of Illinois at Urbana–Champaign, Urbana, Illinois 61801, United States [§]Institute for Molecular Engineering, 5640 South Ellis Avenue, Chicago, Illinois 60637, United States

Materials and instruments:

All reagents were purchased from Acros Organics, Fisher Scientific, Cambridge Chemical Technologies, Chem-Impex International, AK Scientific, TCI America, or Sigma-Aldrich, and used without further purification unless otherwise noted. For the synthetic procedures, dichloromethane (DCM), pyridine, THF, toluene, acetonitrile, DMSO and DMF were stored over activated 4 Å molecular sieves. NMR spectra were recorded using Varian UI400, U500, VXR500, Bruker CB500, or VNS750NB spectrometers in the NMR Laboratory, School of Chemical Science, University of Illinois. Spectra were processed by using MestReNova (v8.1). Mass spectral analyses were provided by the Mass Spectrometry Laboratory, School of Chemical Science, University of Illinois, using ESI on a Waters Micromass Q-Tof spectrometer, FD on a Waters 70-VSE spectrometer. Analytical gel permeation chromatography (GPC) experiments were performed on a Waters system equipped with a Waters 1515 isocratic pump, a Waters 2414 refractive index detector, and a Waters 2998 photodiode array detector. Separations were performed at 50 °C using DMF containing 0.1 M LiBr as the mobile phase. Absolute molecular weights were collected on the above GPC system equipped with an additional miniDAWN TREOS 3-angle laser light scattering detector (MALLS, Wyatt Technology, CA). The detection wavelength of TREOS was 658 nm. The MALLS detector was calibrated using pure toluene and used for the determination of the absolute molecular weights. The molecular weights of all polymers were determined using dn/dc values for each sample calculated offline with the internal calibration system processed by the ASTRA 6 software (version 6.1.1, Wyatt Technology CA). Transmission electron microscopy (TEM) was performed on a JEOL 2100 Cryo TEM, Materials Research Laboratory, University of Illinois at Urbana-Champaign. Dynamic light scattering (DLS) characterization and zeta-potential measurements were performed using a Marvin Instrument Ltd. nanoZS Zetasizer. GPC and DLS data were exported as ASCII files, re-imported into OriginPro2017, plotted, and saved as vector image files (*.ai) in order to be colored/annotated in Adobe Illustrator CC. Fluorescence experiments were performed on a Horiba FluoroMax-4 fluorometer with FluorEssence (v3.5) software. The UV-Vis experiments were performed on Shimadzu UV-2501PC UV-Vis spectrometer with quartz cuvette. The RAW data files were processed using OriginPro2017 and imported into Adobe Illustrator CC.

Synthetic procedure:

1H-Imidazole-1-propanesulfonic acid was synthesized by following a reported procedure.¹

4a was synthesized by following a reported procedure.²

Synthesis of 4b. In a 20-mL glass vial, 3-dimethylamino-1-propyne (200 μ L, 1.86 mmol) and 1-bromopropane (615 mg, 5.0 mmol) were dissolved in MeCN (5 mL), and stirred at 50 °C for 12 h. The crude product was precipitated by adding the solution dropwise to ethyl ether (40 mL), and collected by filtration. The crude product was purified by recrystallization in DCM and hexane at -20 °C to produce 130 mg (34%) of product as a white solid. 1 H NMR (500 MHz, CDCl₃): δ 4.87 (d, J = 2.4 Hz, 2H), 3.66 (m, 2H), 3.50 (s, 6H), 2.99 (t, J = 2.4 Hz, 1H), 1.84 (m, 2H), 1.05 (t, J = 7.3 Hz, 3H). 13 C NMR: (125 MHz, CDCl₃): δ 81.3, 71.5, 65.5, 54.5, 50.6, 16.5, 10.7. High resolution ESI-MS: Calculated for $C_8H_{16}N^+([M]^+)$: 126.1283; obtained 126.1280.

Synthesis of 4c. In a 20-mL glass vial, 3-dimethylamino-1-propyne (200 μL, 1.86 mmol) and 1-bromohexane (825 mg, 5.0 mmol) were dissolved in MeCN (5 mL), and stirred at 50 °C for 12 h. The crude product was precipitated by adding the solution dropwise to ethyl ether (40 mL), and collected by filtration. The crude product was washed with ethyl ether (40 mL) 3 times, and dried under vacuum to afford 265 mg (57%) of the product as a white solid. 1 H NMR (500 MHz, D₂O): δ 4.21 (d, J = 2.2 Hz, 2H), 3.40 (m, 2H), 3.21 (t, J = 2.2 Hz, 1H), 3.14 (s, 6H), 1.75 (m, 2H), 1.28-1.37 (m, 6H), 0.85 (t, J = 7.1 Hz, 3H). 13 C NMR: (125 MHz, CDCl₃): δ 81.2, 71.6, 64.1, 54.4, 50.6, 31.2, 25.9, 22.8, 22.4, 13.9. High resolution ESI-MS: Calculated for $C_{11}H_{22}N^+([M]^+)$: 168.1752; obtained 168.1747.

Synthesis of 4d. In a 20-mL glass vial, 3-dimethylamino-1-propyne (200 μL, 1.86 mmol) and 1-bromononane (1.04 g, 5.0 mmol) were dissolved in MeCN (5 mL), and stirred at 50 °C for 12 h. The crude product was precipitated by adding the solution dropwise to ethyl ether (40 mL) in a 50-mL centrifuge tube, and collected by centrifugation. The crude product was purified by silica column chromatography eluting with 15% (v/v) MeOH in DCM and resulted in 120 mg (22%) of product as a colorless gel-like solid. 1 H NMR (500 MHz, CDCl₃): δ 4.86 (d, J = 2.4 Hz, 2H), 3.65 (m, 2H), 3.50 (s, 6H), 2.92 (t, J = 2.4 Hz, 1H), 1.75 (m, 2H), 1.23-1.40 (m, 12H), 0.87 (t, J = 7.0 Hz, 3H). 13 C NMR: (125 MHz, CDCl₃): δ 81.2, 71.6, 64.1, 54.4, 50.6, 31.8, 29.3, 29.2, 29.1, 26.2, 22.9, 22.6, 14.1. High resolution ESI-MS: Calculated for $C_{14}H_{28}N^{+}([M]^{+})$: 210.2222; obtained 210.2220.

Synthesis of 5b. In a 300-mL round bottom flask, 1,3-propanediol (3.04 g, 40 mmol) was dissolved in dry THF (100 mL), and NaH 60 wt % in mineral oil (1.60 g, 40 mmol) was added slowly with stirring at room temperature. The mixture was stirred at room temperature for 30 min, and propargyl bromide 80 wt % in toluene (2.98 g, 20 mmol) was added. The mixture was refluxed for 12 h. Volatiles were removed under vacuum, and the resulting liquid was added to water (100 mL) and extracted with the mixture of DCM (100 mL) and IPA (20 mL). The organic layer was washed with water (100 mL) twice and brine (100 mL). The solution was dried over Na₂SO₄, and concentrated under vacuum. The crude product was purified by silica column chromatography eluting with 5% (v/v) MeOH in DCM to afford 0.91 g (20%) of product as a pale-yellow liquid. 1 H NMR (500 MHz, CDCl₃): δ 4.17 (d, J = 2.4 Hz, 2H), 3.79 (t, J = 5.8 Hz, 2H), 3.72 (t, J = 5.9 Hz, 2H), 2.46 (t, J = 2.4 Hz, 1H), 2.13 (broad t, 1H), 1.88 (t, 2H). t C NMR: (125 MHz, CDCl₃): t 79.8, 74.8, 68.9, 61.6, 58.6, 32.3. High resolution ESI-MS: Calculated for t C₆H₁₁O₂+ ([M+H]+): 115.0759; obtained 115.0763.

Synthesis of 5c. In a 300-mL round bottom flask, 1,6-hexanediol (4.72 g, 40 mmol) was dissolved in dry THF (100 mL), and NaH 60 wt % in mineral oil (1.60 g, 40 mmol) was added slowly with stirring at room temperature. The mixture was stirred at room temperature for 30 min, and propargyl bromide 80 wt % in toluene (2.98 g, 20 mmol) was added. The mixture was refluxed for 12 h. Volatiles were removed under

vacuum, and the resulting liquid was added to water (100 mL) and extracted with DCM (100 mL). The organic layer was washed with water (100 mL) twice and brine (100 mL). The solution was dried over Na₂SO₄, and concentrated under vacuum. The crude product was purified by silica column chromatography eluting with 20% (v/v) ethyl acetate in DCM to afford 1.0 g (32%)of product as a pale-yellow liquid. 1 H NMR (500 MHz, CDCl₃): δ 4.15 (d, J = 2.4 Hz, 2H), 3.66 (t, J = 6.5 Hz, 2H), 3.53 (t, J = 6.5 Hz, 2H), 2.44 (t, J = 2.4 Hz, 1H), 1.60 (t, 4H), 1.47 (t, 4H), 1.26 (t, 1H). t C NMR: (125 MHz, CDCl₃): t 80.2, 74.4, 70.4, 63.2, 58.3, 32.9, 29.7, 26.2, 25.8. High resolution ESI-MS: Calculated for t C₉H₁₇O₂+ ([M+H]+): 157.1229; obtained 157.1234.

Synthesis of 5d. In a 300-mL round bottom flask, 1,9-nonanediol (6.40 g, 40 mmol) was dissolved in dry THF (100 mL), and NaH 60 wt % in mineral oil (1.60 g, 40 mmol) was added slowly with stirring at room temperature. The mixture was stirred at room temperature for 30 min, and propargyl bromide 80 wt % in toluene (2.98 g, 20 mmol) was added. The mixture was refluxed for 12 h. Volatiles were removed under vacuum, and the resulting liquid was added to water (100 mL) and extracted with DCM (100 mL). The organic layer was washed with water (100 mL) twice and brine (100 mL). The solution was dried over Na₂SO₄, and concentrated under vacuum. The crude product was purified by silica column chromatography eluting with 30% (v/v) ethyl acetate in hexane to afford 2.8 g (70%) of product as a pale-yellow liquid. 1 H NMR (500 MHz, CDCl₃): δ 4.15 (d, J = 2.4 Hz, 2H), 3.66 (t, J = 6.6 Hz, 2H), 3.52 (t, J = 6.6 Hz, 2H), 2.44 (t, J = 2.4 Hz, 1H), 1.59 (t, 4H), 1.27-1.33 (t, 11H). t C NMR: (125 MHz, CDCl₃): t 80.0, 74.1, 70.3, 63.0, 60.4, 58.0, 32.8, 29.5, 29.4, 29.3, 26.1, 25.7. High resolution ESI-MS: Calculated for t C₁₂H₂₃O₂ + ([M+H]⁺): 199.1698; obtained 199.1701.

Synthesis of 5e. In a 300-mL round bottom flask, 6-heptyn-1-ol (2.24 g, 20 mmol) and CBr₄ (6.6 g, 20 mmol) were dissolved in DCM (100 mL), and triphenylphosphine (5.24 g, 20 mmol) in DCM (50 mL) was added dropwise at 0 °C with stirring. The mixture was stirred at room temperature overnight. Volatiles were removed under vacuum, and hexane (80 mL) and ethyl ether (20 mL) were added and stirred for 30 min. The insoluble solid was removed by filtration and the filtrate was concentrated under vacuum, and purified by silica column chromatography eluting with pentane to afford 1.9 g (54%) of product as a pale-yellow liquid. 1 H NMR (500 MHz, CDCl₃): δ 3.44 (t, J = 6.8 Hz, 2H), 2.24 (m, 2H), 1.98 (t, J = 2.6 Hz, 2H), 1.89 (m, 1H), 1.59 (m, 4H). 13 C NMR: (125 MHz, CDCl₃): δ 84.4, 68.8, 33.8, 32.5, 27.8, 27.5, 18.5.

Synthesis of 6b. In a 100-mL round bottom flask, **5e** (1.05 g, 6.0 mmol) and Na₂SO₃ (3.78 g, 30 mmol) were refluxed in the mixture of water (20 mL) and EtOH (20 mL) under N₂ for 24 h. Insoluble inorganic salts were removed by filtration, and volatiles in the solution were removed under vacuum. The resulting solid was washed with acetone (13 mL) and MeOH (1 mL) and the organic solution was concentrated to about 2 mL. To the concentrated solution was added ethyl ether (13 mL) to give precipitate which was filtered off and washed with ethyl ether (14 mL) twice to afford 0.80 g (67%) of product as a white solid. ¹H NMR (500 MHz, CD₃OD): δ 2.73 (t, J = 2.5 Hz, 1H), 2.39 (m, 2H), 2.11 (m, 2H), 1.53 (m, 2H), 1.38 (m, 4H). ¹³C NMR: (125 MHz, CD₃OD): δ 85.2, 71.9, 52.0, 28.5, 28.2, 25.3, 18.3. High resolution ESI-MS: Calculated for C₇H₁₁O₃S⁻ ([M]⁻): 175.0429; obtained 175.0437.

Synthesis of 5f. In a 200-mL round bottom flask, **5d** (1.98g, 10 mmol) and CBr₄ (3.81 g, 1.15 mmol) were dissolved in DCM (50 mL), and triphenylphosphine (3.01 g, 1.15 mmol) in DCM (20 mL) was added dropwise at 0 °C with stirring. The mixture was stirred at room temperature overnight. Volatiles were removed under vacuum, and a mixture of hexane (40 mL) and ethyl ether (10 mL) was added and stirred for 30 min. Insoluble solid was removed by filtration and the filtrate was concentrated under vacuum and purified by silica column chromatography eluting with 20% (v/v) DCM in hexane to afford 2.1g (81%) of product as a pale-yellow liquid. ¹H NMR (500 MHz, CDCl₃): δ 4.16 (d, J = 2.4 Hz, 2H), 3.53 (t, J = 6.5 Hz, 2H), 3.42 (t, J = 6.8 Hz, 2H), 2.44 (t, J = 2.3 Hz, 1H), 1.87 (m, 2H), 1.59 (m, 2H), 1.31-1.47 (m, 10H). ¹³C NMR: (125 MHz, CDCl₃): δ 80.3, 74.3, 70.5, 58.3, 34.3, 33.1, 29.7, 29.6, 29.5, 28.9, 28.4, 26.3. High resolution ESI-MS: Calculated for C₁₂H₂₀OBr⁺ ([M+H]⁺): 259.0688; obtained 259.0698 and 261.0703.

Br
$$\frac{Na_2SO_3}{H_2O, EtOH, reflux}$$
 0 6c SO_3Na_3

Synthesis of 6c. In a 100-mL round bottom flask, 5f (0.52 g, 2.0 mmol) and Na_2SO_3 (2.5 g, 20 mmol) were refluxed in water (10 mL) and EtOH (10 mL) under N_2 for 48 h. Volatiles were removed under vacuum, and the resulting solid was washed with acetone (20 mL) 3 times. The acetone solutions were combined, and concentrated to around 2-3 mL under vacuum. To the resulting solution was added ethyl ether (13 mL) to give a precipitate, which was filtered off and washed with ethyl ether (14 mL) twice to afford 0.21 g (37%) of product as a white solid. ¹H NMR (500 MHz, CD_3OD): δ 4.07 (d, J = 2.3 Hz, 2H), 3.39 (m, 3H), 2.37 (m,

2H), 1.44-1.55 (m, 4H), 1.2-1.27 (m, 10H), 1.59 (m, 2H), 1.31-1.47 (m, 10H). ¹³C NMR: (125 MHz, CD₃OD): δ 81.2, 77.6, 69.8, 57.9, 52.2, 29.6, 29.1, 26.3, 25.8. High resolution ESI-MS: Calculated for $C_{12}H_{21}O_4S^-$ ([M] $^-$): 261.1161; obtained 261.1159.

7 was synthesized by following a reported procedure.³

BTTAA was synthesized by following a reported procedure.4

Monomers M1, M2, M3, M4 and M5 were synthesized by following reported procedures.5-7

General synthetic procedure of polymer P1. In a 20-mL glass vial, monomer M1 and M2 were dissolved in DCM. With fast stirring, Grubbs 3rd generation catalyst was added into the solution under N₂, and the solution was stirred at room temperature for 5-15 min (the time depended on degree of polymerization desired). Butyl vinyl ether was added and stirred for another 10 min. Volatiles were removed under reduced pressure. The polymer was used in the next step without further purification.

General synthetic procedure of *N*-butylimidazolium functionalized polymer P2. In a 20-mL glass vial, 50 mg of P1, DMF (1 mL) and *N*-butylimidazole (200 μ L) were added. The reaction vial was sealed and heated to 50 °C for 24 h. The resulting DMF solution was added into cold ethyl ether (13 mL in a 15-mL centrifuge tube) to precipitate the functionalized polymer. The precipitate was isolated by centrifugation and the supernatant was discarded. The precipitate was redissolved in MeOH (1 mL) and the solution was added to ethyl ether (14 mL), and the precipitate was isolated by centrifugation. This process was repeated 3 times. The resulting gel-like solid was dissolved and stirred in TFA (2 mL) at room temperature for 3 h. The TFA solution was precipitated in ethyl ether (13 mL), and the precipitate was isolated by centrifugation. The resulting gel-like solid was dissolved in water (3 mL) and dialyzed against 1 M NaCl aqueous solution for 8 h, and water for 48 h. Yields typically range from 80%-90% due to the loss during precipitation and dialysis.

Synthetic procedure of zwitterionic polymer P3. In a 20-mL glass vial, 50 mg of P1-40-20 was dissolved in DMF (1 mL), and DIPEA (200 μ L) and 1*H*-Imidazole-1-propanesulfonic acid (200 mg) was added. The reaction vial was sealed and heated to 50 °C for 24 h. The resulting DMF solution was added into cold ethyl ether (13 mL in a 15-mL centrifuge tube) to precipitate the polymer. The precipitate was dissolved in water (3 mL) and dialyzed against water for 24 h to remove excess starting materials. The resulting solution was lyophilized, and the polymer was stirred in TFA (2 mL) at room temperature for 3 h. The TFA solution was precipitated in ethyl ether (13 mL), and the precipitate was isolated by centrifugation. The resulting gel-like solid was dissolved in water (3 mL) and dialyzed against 1 M NaCl aqueous solution for 8 h, and water for 48 h. Yields typically range from 80%-90% due to the loss during precipitation and dialysis.

Synthetic procedure of methylimidazolium functionalized polymer P4. In a 20-mL glass vial, 50 mg of P1 was dissolved in DMF (1 mL) and N-methylimidazole (200 μ L). The reaction vial was sealed and heated to 50 °C for 24 h. The resulting DMF solution was added into cold ethyl ether (13 mL in a 15-mL centrifuge tube) to precipitate the polymer. The precipitate was isolated by centrifugation and the supernatant was discarded. The precipitate was redissolved in MeOH (1 mL) and the solution was added to ethyl ether (14 mL), and the precipitate was isolated by centrifugation. This process was repeated for 3 times. The resulting gel-like solid was dissolved and stirred in TFA (2 mL) at room temperature for 3 h. The TFA solution was precipitated in ethyl ether (13 mL), and the precipitate was isolated by centrifugation. The

resulting gel-like solid was dissolved in water (3 mL) and dialyzed against 1 M NaCl aqueous solution for 8 h, and water for 48 h. Yields typically range from 80%-90% due to the loss during precipitation and dialysis.

P5 and P6 were synthesized through the same procedure as P1 and P2

Synthetic procedure of azido polymer P7. In a 20-mL glass vial, 100 mg of P5 was dissolved in DMF (2 mL) and NaN_3 (130 mg 2 mmol) was added. The reaction vial was sealed and heated to 50 °C for 24 h. DCM (13 mL) was added to the DMF solution, and insoluble inorganic salts were removed by filtration. DCM was removed under vacuum, and the DMF solution was used in the next step without further purification.

Synthetic procedure of anionic polymer P8. The DMF solution of P7 was added CuBr (14.4 mg, 0.1 mmol), 6c (0.13 g, 0.4 mmol) and PMDETA (30 μ L) under N₂. The mixture was stirred at 50 °C under N₂ for 12 h. Water (1 mL) was added gradually during the reaction to keep the polymer soluble. The mixture was dialyzed against water for 12 h. 1-2 g of chelating resin (Lewatit® TP 207) was added to the aqueous polymer solution and gently stirred for 3 h to remove Cu ion, and the resin was removed by filtration. This process was repeated 3 times to completely remove Cu. The solvent was removed under vacuum and the resulting gel-like solid was dissolved and stirred in TFA (2 mL) at room temperature for 3 h. The TFA solution was precipitated in ethyl ether (13 mL), and the precipitate was isolated by centrifugation. The resulting gel-like solid was dissolved in water (3 mL) and dialyzed against 1 M NaCl aqueous solution for 8 h and water for 48 h.

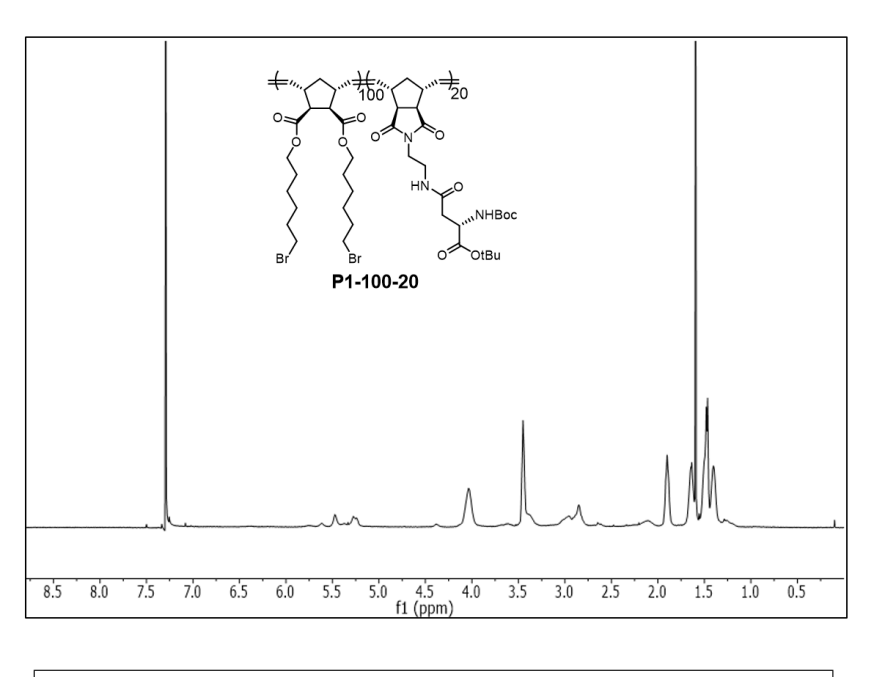
Synthetic procedure of P9. In a 20-mL glass vial, monomer M2 (89.6 mg, 0.2 mmol), M4 (63.6 mg, 0.2 mmol) and M5 (55.4 mg, 0.2 mmol) were dissolved in DCM (6 mL). With fast stirring, 400 μ L of a solution of Grubbs 3rd generation catalyst in DCM was added to the mixture under N₂, and the solution was stirred at room temperature for 6 min. Butyl vinyl ether (1 mL) was added and stirred for another 10 min. Volatiles were removed under reduced pressure. The polymer was redissolved in DCM (1 mL) and added into cold ethyl ether (13 mL in a 15-mL centrifuge tube) to precipitate the polymer. The precipitate was isolated by centrifugation and washed with ethyl ether (15 mL) 3 times. The polymer was dried under vacuum.

Synthetic procedure of P10. In a 20-mL glass vial, **P9** from the previous step was dissolved in DCM (5 mL) and nitrobenzene (0.1 mL). **Triallyl-Tris** (0.3 mL) was added, and stirred at 40 °C for 12 h. Volatiles were removed under vacuum, and the viscous residue was redissolved in DCM (1 mL). The solution was precipitated in a 2:1 (v/v) mixture of cold ether-hexanes (-15 °C) in a 15-mL polypropylene centrifuge tube, and the solid was further washed with ethyl ether (15 mL) 3 times. The polymer was dried under vacuum.

Synthetic procedure of P11. In a 20-mL vial, 100 mg of P10 was resuspended in a mixture of acetone (12 mL) and water (3 mL) with stirring. N-methylmorpholine N-oxide (1mL, 50 wt%, aq) and K_2OsO_4 (2 mg) were added to the mixture. The vial was loosely capped and stirred at 40 °C for 24 h, and water (2-3 mL) was added during the reaction to keep the polymer soluble. The resulting solution was purified by dialysis against water for 12 h. TFA was added to the dialyzed solution to bring the pH below 1, and stirred at 35 °C for 12 h to deprotect the amino acid groups. The solution was dialyzed against water for 6 h to remove TFA. The solution was stirred in 0.2 M NaOH aqueous solution to hydrolyze ester groups. The solution was dialyzed against water for 48 h, and lyophilized, resulting in an off-white powder.

General synthetic procedure of SCNP. The parent polymer was dissolved in water/PBS buffer to reach the concentration at 20 μ M. With fast stirring, CuSO₄ was added as 10 mM aqueous solution, and the mixture was stirred at room temperature for 12 h. The solution was used directly for the reaction without further purification.

Polymer characterization:



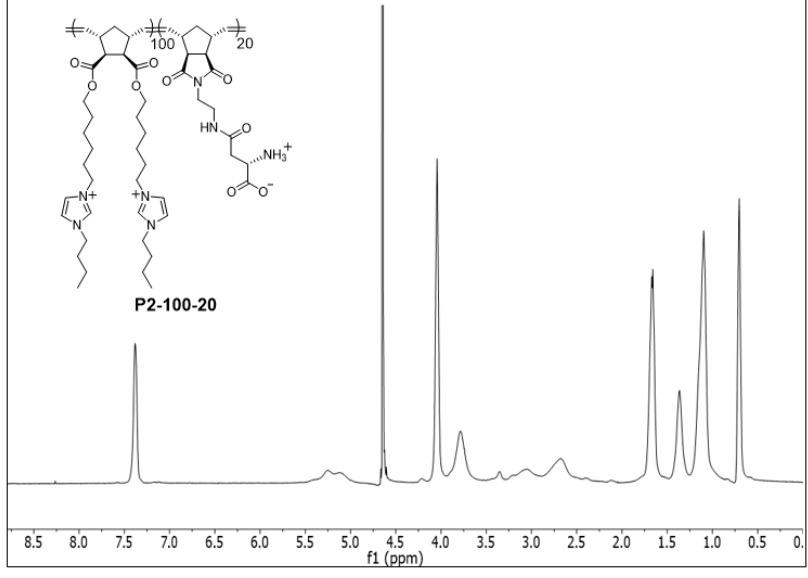


Figure S2. Representative structure and 1 H NMR spectrum of imidazolium functionalized P2-100-20 in $D_{2}O$.

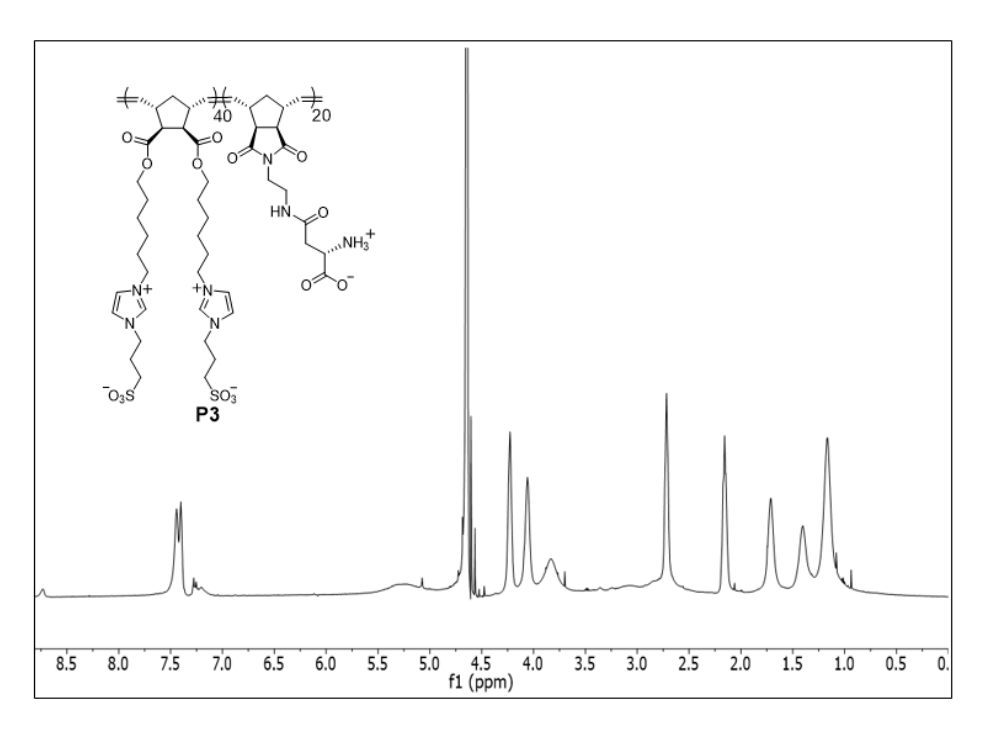


Figure S3. Structure and ¹H NMR spectrum of P3 in D₂O.

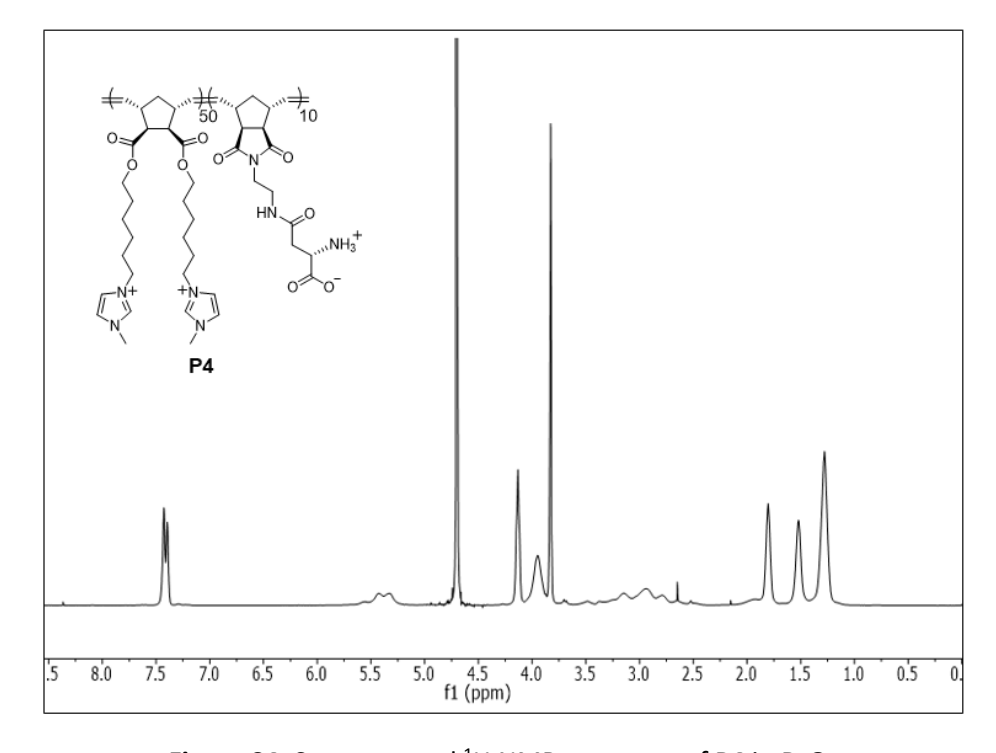


Figure S4. Structure and ^1H NMR spectrum of P4 in D $_2\text{O}$.

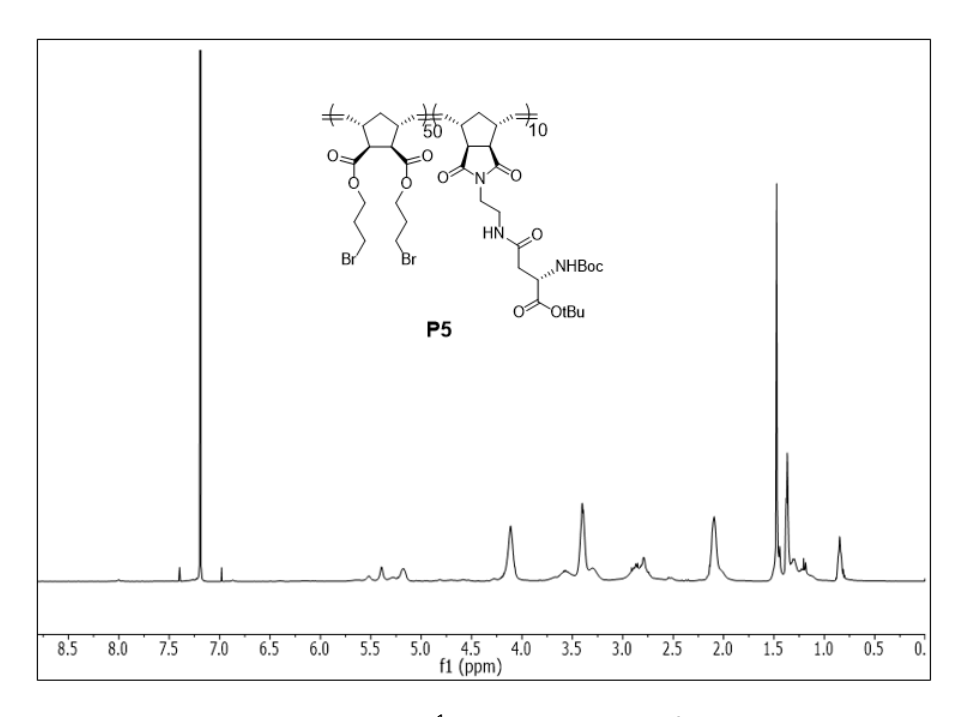


Figure S5. Structure and ¹H NMR spectrum of P5 in CDCl₃.

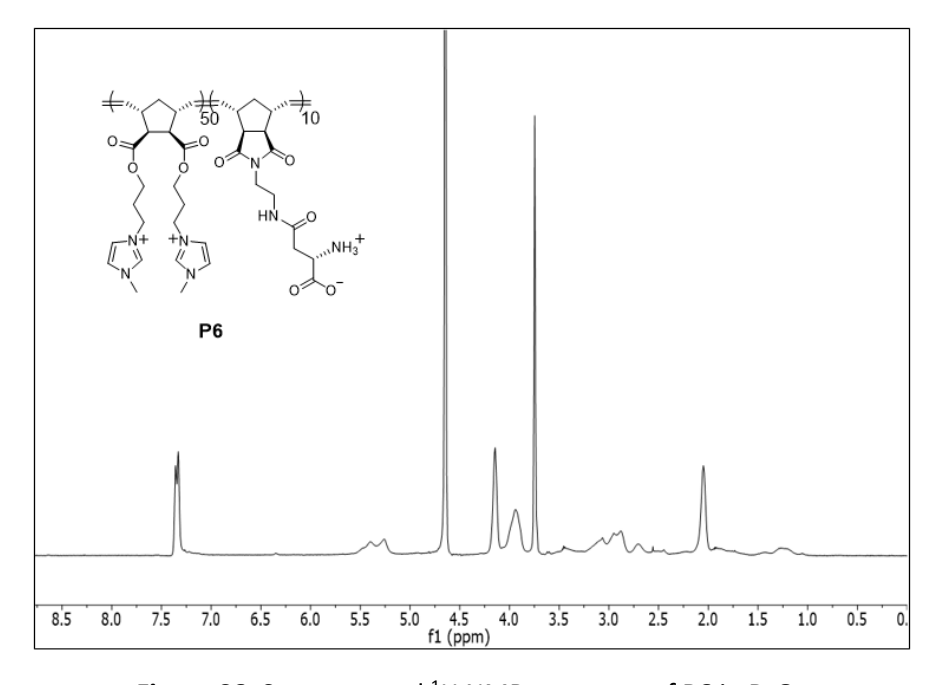


Figure S6. Structure and ¹H NMR spectrum of **P6** in D₂O.

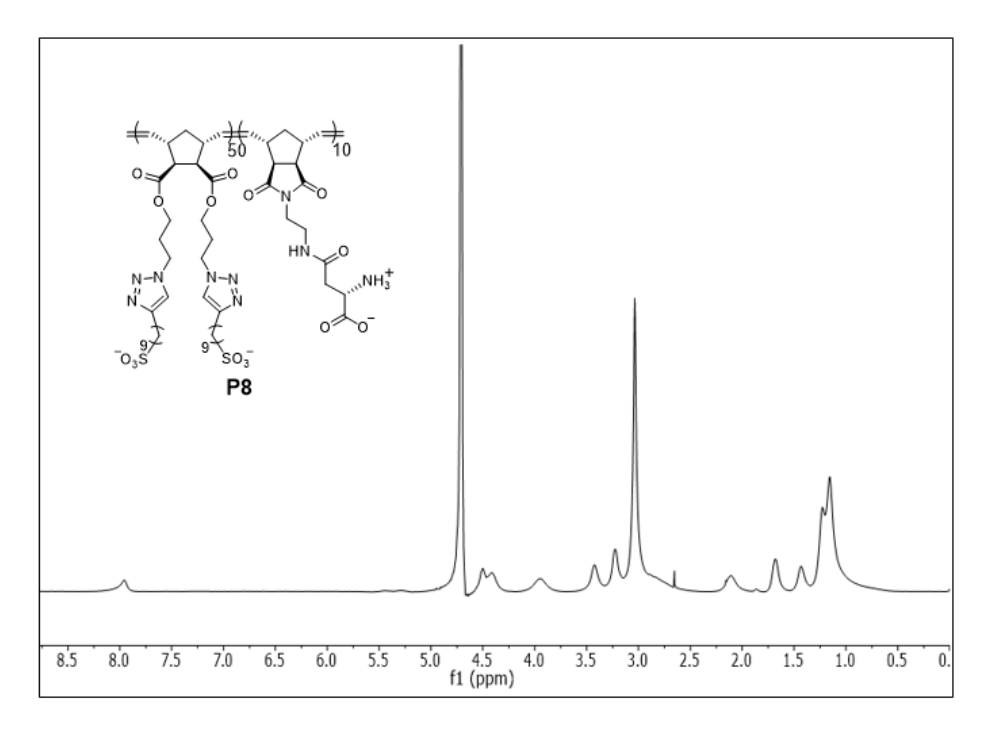


Figure S7. Structure and 1H NMR spectrum of P8 in D_2O .

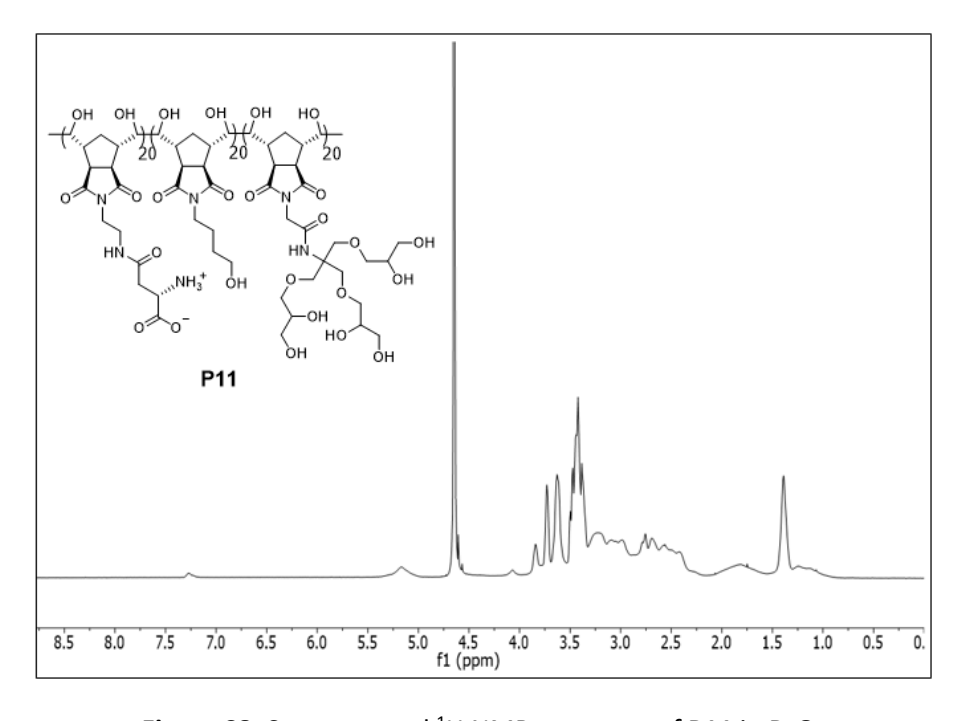


Figure S8. Structure and ${}^{1}H$ NMR spectrum of P11 in D2O.

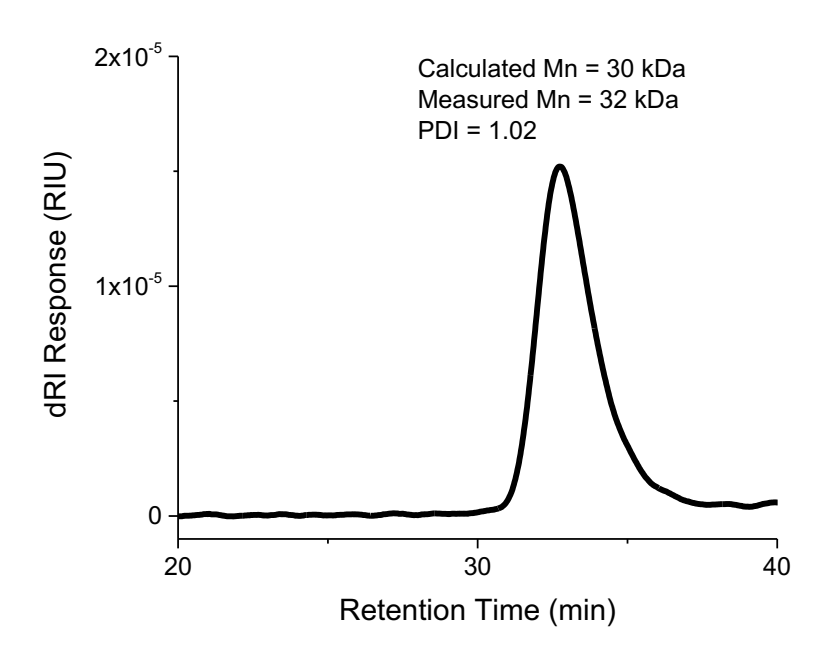


Figure S9. Representative GPC elution curve of **P1-50-10**.

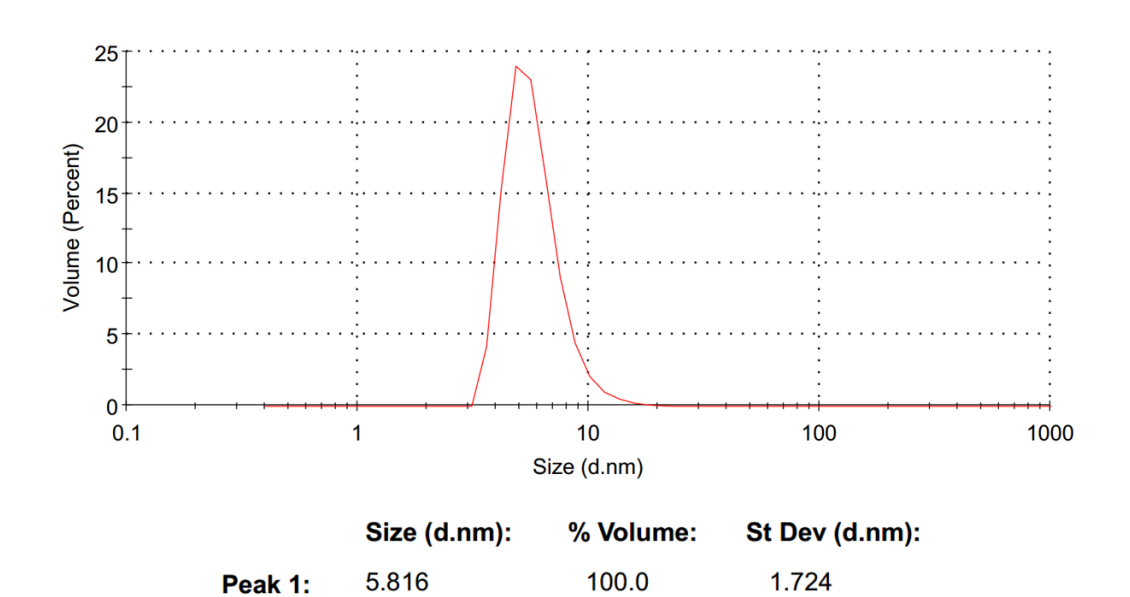


Figure S10. Representative DLS of SCNP-2a in water.

Kinetics:

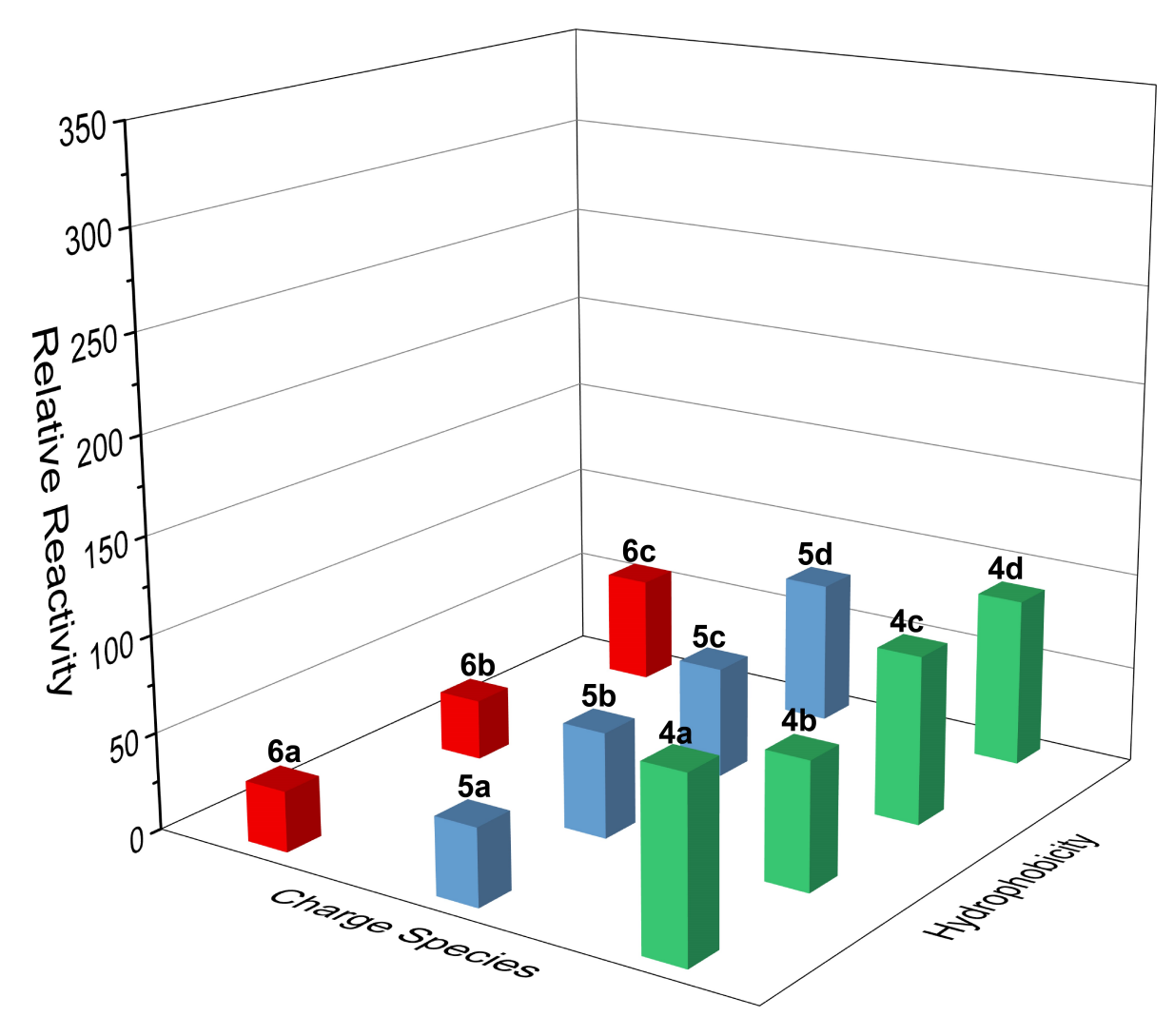


Figure S11. Reaction rates of fluorogenic CuAAC click reactions performed with **1** (20 μ M), alkyne substrates (40 μ M), sodium ascorbate (2 mM) and **BTTAA-Cu** (20 μ M) in PBS buffer (pH = 7.4).

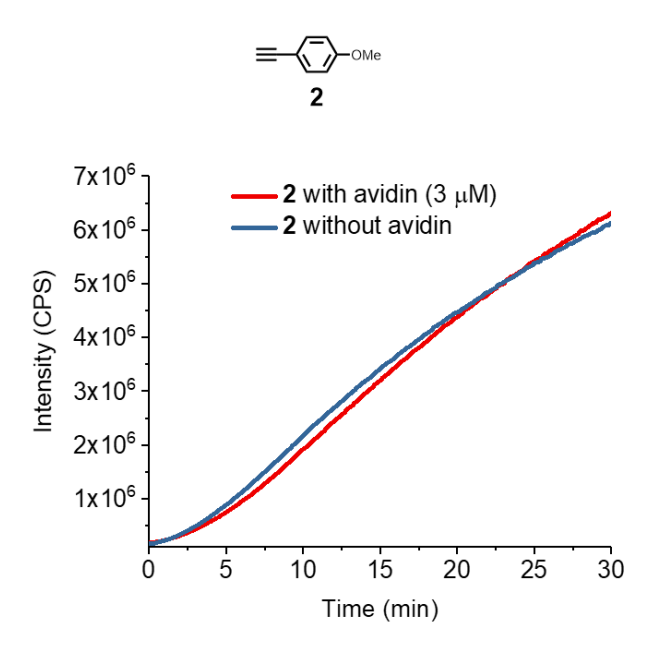


Figure S12. Fluorogenic reaction kinetics of **2** (10 μ M) with or without avidin (3 μ M). The reactions are catalyzed by **SCNP-2a** (4 μ M) with **1** (20 μ M) and sodium ascorbate (2 mM) in PBS

ITC Study:

ITC measurements were performed at 25 °C on a MicroCal VP-ITC calorimeter. A typical experiment consisted of titrating 10 μ L of **6c** (10 mM) from a 250 μ L syringe (stirred at 300 rpm) into a sample cell containing 1.42 mL of **SCNP-2a** solution (10 μ M) with a total of 28 injections (2 μ L for the first injection and 10 μ L for the remaining injections). The initial delay prior to the first injection was 300 s. The duration of each injection was 20.5 s and the delay between injections was 400 s. All the sample were dissolved in Milli-Q water, and data analysis was carried out with OriginPro2017.

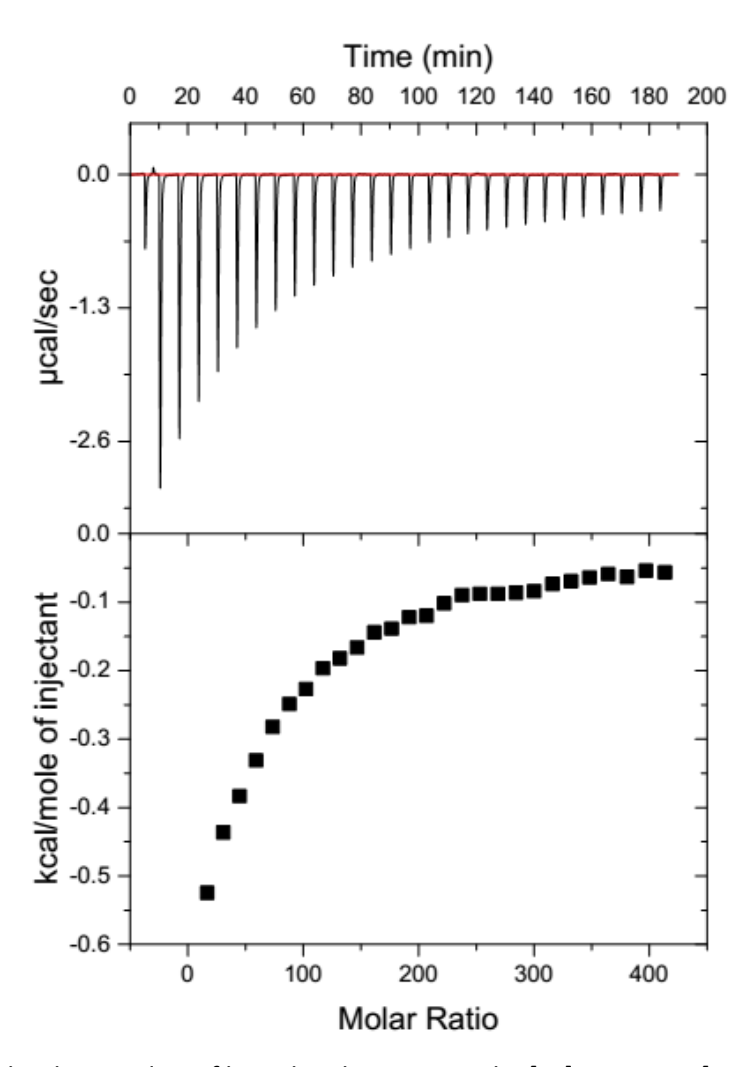


Figure S13. ITC binding studies of ligand with nanoparticle; [6c] = 10 mM, [SCNP-2a] = 10 μ M.

Molecular dynamics simulation methods:

All-atom molecular topologies and optimized geometries of the polymer and five small molecules were generated using the freely available Automated Topology Builder (ATB) (http://atb.uq.edu.au).8 Optimized geometries were constructed by steepest descent energy minimization. For the polymer, smaller fragments were generated first and assembled to construct the full structure. Bonded and van der Waals terms of the molecular topology were modeled using the GROMOS 54A7 force field,9 and partial charges assigned by semi-empirical quantum mechanical calculations conducted using the MOPAC method.¹⁰ Molecular dynamics simulations were performed in GROMACS 4.6.¹¹⁻¹² Lennard-Jones interactions were shifted smoothly to zero at 1.4 nm, and dispersion interactions between unlike atoms specified by Lorentz-Berthelot combining rules. 13 Coulomb interactions were treated by Particle Mesh Ewald (PME) with a real-space cutoff of 1.4 nm and a 0.12 nm reciprocal-space grid spacing. ¹⁴ Bond lengths were fixed to their equilibrium values using the LINCS algorithm. 15 SPC water molecules are used as the solvent for each simulation.¹⁶ Temperature was maintained at 300 K using a Nosé-Hoover thermostat¹⁷ and pressure at 1.0 bar using an isotropic Parrinello-Rahman barostat. 18 Newton's equations of motion were integrated using the leap-frog algorithm¹⁹ with time step of 2 fs. One 100 ns simulation is conducted first to fold the stretched polymer into a collapsed sphere, after which five simulations for different small molecules were conducted independently with the same initial folded polymer sphere and random distributed small molecules in a box with the size of $11 \times 11 \times 11$ nm³. Each simulation lasts for 20 ns, and the analysis is conducted over the terminal 10 ns over which period the ratio of substrate molecules inside the substrate to those outside has reached a stable value (Figure S14). A substrate molecule is defined to be bound within the nanoparticle if the center of mass (COM) distance between the substrate molecule and the nanoparticle is smaller than 3 nm, which is the typical radius of the nanoparticle.

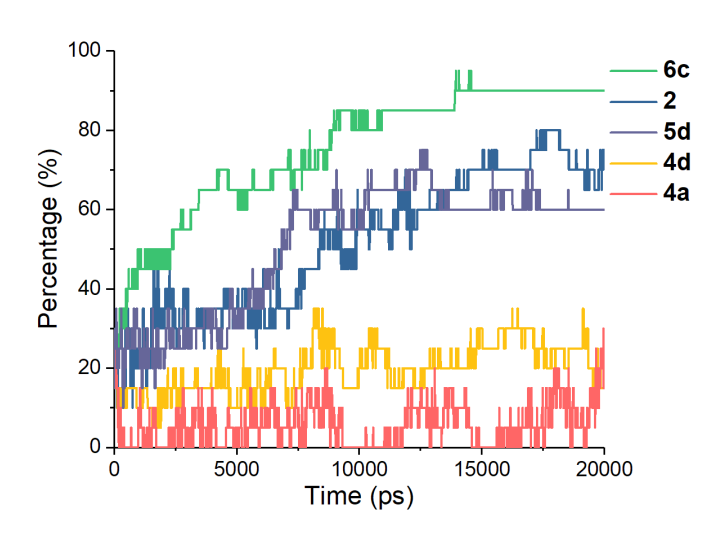


Figure S14. Kinetics of small molecules distributions during the binding simulation.

References.

- 1. Wu, Z.; Li, Z.; Wu, G.; Wang, L.; Lu, S.; Wang, L.; Wan, H.; Guan, G. *Ind. Eng. Chem. Res.* **2014**, *53*, 3040.
- 2. Yao, Z.; Yang, Y.; Chen, X.; Hu, X.; Zhang, L.; Liu, L.; Zhao, Y.; Wu, H.-C. Anal. Chem. 2013, 85, 5650.
- 3. Nainar, S.; Kubota, M.; McNitt, C.; Tran, C.; Popik, V. V.; Spitale, R. C. *J. Am. Chem. Soc.* **2017**, *139*, 8090.
- 4. Besanceney-Webler, C.; Jiang, H.; Zheng, T.; Feng, L.; Soriano del Amo, D.; Wang, W.; Klivansky, L. M.; Marlow, F. L.; Liu, Y.; Wu, P. *Angew. Chem. Int. Ed.* **2011**, *50*, 8051.
- 5. Bai, Y.; Feng, X.; Xing, H.; Xu, Y.; Kim, B. K.; Baig, N.; Zhou, T.; Gewirth, A. A.; Lu, Y.; Oldfield, E.; Zimmerman, S. C. *J. Am. Chem. Soc.* **2016**, *138*, 11077.
- 6. Bai, Y.; Xing, H.; Vincil, G. A.; Lee, J.; Henderson, E. J.; Lu, Y.; Lemcoff, N. G.; Zimmerman, S. C. *Chem. Sci.* **2014**, *5*, 2862.
- 7. Bai, Y.; Xing, H.; Wu, P.; Feng, X.; Hwang, K.; Lee, J. M.; Phang, X. Y.; Lu, Y.; Zimmerman, S. C. *ACS Nano* **2015**, *9*, 10227.
- 8. Malde, A. K.; Zuo, L.; Breeze, M.; Stroet, M.; Poger, D.; Nair, P. C.; Oostenbrink, C.; Mark, A. E. *J. Chem. Theory Comput.* **2011**, *7*, 4026.
- 9. Schmid, N.; Eichenberger, A. P.; Choutko, A.; Riniker, S.; Winger, M.; Mark, A. E.; van Gunsteren, W. F. *Eur. Biophys. J.* **2011**, *40*, 843.
- 10. Stewart, J. J. P. J. Comput. Aided Mol. Des. 1990, 4, 1.
- 11. Hess, B.; Kutzner, C.; van der Spoel, D.; Lindahl, E. J. Chem. Theory Comput. 2008, 4, 435.
- 12. Pronk, S.; Páll, S.; Schulz, R.; Larsson, P.; Bjelkmar, P.; Apostolov, R.; Shirts, M. R.; Smith, J. C.; Kasson, P. M.; van der Spoel, D.; Hess, B.; Lindahl, E. *Bioinformatics* **2013**, *29*, 845.
- 13. Allen, M. P.; Tildesley, D. J. Computer Simulation of Liquids; Clarendon Press: New York, 1987; p 385.
- 14. Essmann, U.; Perera, L.; Berkowitz, M. L.; Darden, T.; Lee, H.; Pedersen, L. G. *J. Chem. Phy.* **1995**, *103*, 8577.
- 15. Hess, B.; Bekker, H.; Berendsen, H. J. C.; Fraaije, J. G. E. M. J. Comput. Chem. 1997, 18, 1463.
- 16. Berendsen, H.; Postma, J.; van Gunsteren, W.; Hermans, J. Interaction models for water in relation to protein hydration. In Intermolecular Forces; Pullman, B., Ed.; Reidel: Dordrecht, 1981; pp 331–342.
- 17. Nosé, S. J. Chem. Phys. **1984**, 81, 511.
- 18. Parrinello, M.; Rahman, A. J. Appl. Phys. 1981, 52, 7182.
- 19. Hockney, R. W.; Eastwood, J. W. Computer Simulation Using Particles; CRC Press: Boca Raton, 2010.